People`s Democratic Republic of Algeria
Ministry of Higher Education and Scientific Research
University of Echahid Hamma Lakhdar - El Oued

Faculty of Technology
Department of electrical engineering

Dissertation
ACADEMIC MASTER
Domain: Science and Technology
Division: Telecommunications
Specialty: Telecommunications Systems

Presented by:

- AOUINATE Amina
- CHENNOUF Anhar

Entitled:

Optimization of solar cell performance through numerical simulation

Dissertation Submitted in Partial Fulfillment of the Requirements for the Master Degree in Telecommunications Systems

Board of Examiners:

Dr. HIMA Abdelkader	**Chairman**
Dr. KATEB Mohamed Nadjib	**Supervisor**
Dr. MOUSSI Fouaze	**Examiner**

Academic Year: 2023/2024

Acknowledgment

Praise be to God who granted me success in completing this work. I extend my deepest gratitude and appreciation to everyone who supported me throughout my academic journey.

I would like to express my sincere thanks to my esteemed professors, who generously shared their valuable knowledge and offered me their insightful guidance. Their direction had a profound impact on enriching my understanding and developing this research. Thank you for your time, effort, and patience.

I am also deeply grateful to my dear parents, who have been my greatest support, providing me with emotional and financial assistance throughout my studies. Your unwavering presence by my side at every step of my life has been the driving force behind this achievement.

I would also like to extend my thanks to my friends and colleagues, who accompanied me on this journey and were a constant source of support and encouragement.

Finally, I wish to thank everyone who contributed, whether directly or indirectly, to the completion of this dissertation. I hope that the result of my efforts meets the expectations of all.

Dedication

To my dear parents,
who have always been a source of strength and support, and who never hesitated to offer me advice and guidance. I extend my deepest gratitude for the love and care you have given me, as you were the foundation upon which this success was built.

To my esteemed teachers,
who generously shared their knowledge and experience, and continuously guided me in the right direction. Thank you for your unwavering support, belief in my abilities, and motivating me to strive for excellence.

To my dear friends,
who stood by my side at every step, never hesitating to offer help and encouragement. Thank you for always being there, as your support was a driving force in overcoming challenges and achieving this accomplishment.

And finally, to myself,
for being patient and persistent, and for not giving up despite the hardships. I dedicate this success to myself and take pride in what I have achieved.

Abstract

This thesis discusses semiconductor materials and solar cell technologies, focusing on their properties, operating principles, and optimization strategies. The basic electronic properties of semiconductors are discussed, highlighting the role of crystal structures in materials such as silicon, germanium, and gallium arsenide (GaAs). The photovoltaic effect and different types of solar cells are explained, focusing on the conversion of solar energy into electricity and the advantages of emerging technologies. The SCAPS-1D simulation program, a tool for modeling and designing solar cell performance, is studied. Solar cells made of gallium arsenide, especially its p-i-n structure, are studied, showing that optimized parameters can enhance the efficiency to 30.04%. Overall, this paper emphasizes the critical role of semiconductor materials in renewable energy and the importance of design improvements to improve solar cell performance, paving the way for next-generation solar technologies.

الملخص

يتناول هذا البحث المواد شبه الموصلة وتقنيات الخلايا الشمسية، مع التركيز على خصائصها ومبادئ تشغيلها واستراتيجيات التحسين. تم التطرق الى الخصائص الإلكترونية الأساسية لأشباه الموصلات، وتسليط الضوء على دور الهياكل البلورية في مواد مثل السيليكون والجرمانيوم وزرنيخيد الغاليوم (GaAs). توضيح التأثير الكهروضوئي وأنواع الخلايا الشمسية المختلفة، مع التركيز على تحويل الطاقة الشمسية إلى كهرباء ومزايا التقنيات الناشئة. دراسة برنامج محاكاة SCAPS-1D، وهو أداة لنمذجة أداء الخلايا الشمسية وتصميمها. دراسة الخلايا الشمسية المصنوعة من زرنيخيد الغاليوم، وخاصة هيكلها p-i-n، مما يدل على أن المعلمات المحسنة يمكن أن تعزز الكفاءة إلى 30.04%. وبشكل عام، يؤكد هذا البحث على الدور الحاسم للمواد شبه الموصلة في الطاقة المتجددة وأهمية تحسينات التصميم لتطوير أداء الخلايا الشمسية، وتمهيد الطريق لتقنيات الطاقة الشمسية من الجيل التالي.

Table of Contents

CHAPTER 1: Electronic properties of semiconductor materials

1.1 Introduction 3
1.2 Crystal structure 3
1.3 Element semiconductors 4
1.4 Energy Bands 4
1.5 Conduction in metals, semiconductors, and insulators 6
1.5.a Metals 6
1.5.b Semiconductors 6
1.5.c Insulators 7
1.6 Intrinsic semiconductors 7
1.7 Extrinsic semiconductors 9
1.8 Currents in the Semiconductor 12
1.9 Generation of Excess Carriers by Light 13
1.10 Recombination of Excess Carriers 14
1.11 Gallium Arsenide (GaAs): Properties, Uses 14
1.11.a Structure of GaAs 15
1.11.b Properties of GaAs 15
1.11.c Use of GaAs 15
1.12 conclusion 16
Chapter 1 references 17

CHAPTER 2: Solar cells fundamentals device

2.1 introduction 19
2.2 Solar radiation 19
2.3 Transfer of energy from the photon to the electron 20
2.4 Principle of Operation of a Solar Cell 21
2.5 Electrical characteristics 23
2.5.1 The ideal solar cell 23
2.5.2 Solar cell characteristics in practice 25
2.6 Types of Solar Cells 27
2.7 Conclusion 28
Chapter 2 references 29

Chapter 3: SCAPS-1D program

3.1 Introduction 31
3.2 Fundamental equations in semiconductors 31
3.3 About SCAPS 31
3.4 SCAPS interface 33
3.5 Working point 34
3.6 Spectrum and illumination: 34
3.7 Select the measurement(s) to simulate 35
3.8 Define the problem 35
3.9 Change parameters: 36
3.10 Start the calculation(s) 37
3.11 Display the simulated curves: 38
3.12 Conclusion 38
Chapter 3 references 39

Chapter 4: Simulation and results

4.1 Introduction 41
4.2 GaAs solar cell 41
4.3 Device structure of p-i-n GaAs solar cell and simulation parameters 41
4.4 solar cell performance 43
4.5 Optimization of GaAs solar cell performance 44
4.5.a Optimization of acceptor concentrations of GaAs solar cell p-layer 44
4.5.b Optimization of donor concentrations of solar cell n-layer 45
4.5.c Optimization of thicknesses of solar cell p-layer 46
4.5.d Optimization of thicknesses of solar cell i-layer 47
4.5.e Optimization of thicknesses of solar cell n-layer 48
4.5 Conclusion 50
Chapter 4 references 51

List of figures

Chapter 1: Electronic properties of semiconductor materials

Figure 1.1 (a) Diamond lattice, (b) Zinc blende lattice……3
Figure 1.2 Formation des bandes d'énergie pour les électrons d'atomes de Si arrangés en mailles cristallines de type diamant…….5
Figure 1.3 Schematic energy band representations of (a) a conductor with two possibilities (either the partially filled conduction band shown at the upper portion or the overlapping bands shown at the lower portion), (b) a semiconductor, (c) an insulator……6
Figure 1.4 Intrinsic semiconductor: (a) Schematic band diagram, (b) Density of states, (c) Fermi distribution function, (d) Carrier concentration……..…..8
Figure 1.5 Schematic bond pictures for (a) n-type Si with donor (arsenic) and (b) p-type Si with acceptor (boron)……..……..10
Figure 1.6 (a) Schematic energy band representation of extrinsic n-type, (b) p-type semiconductors…….11
Figure 1.7 The structure of Gallium arsenide wafer…….15

Chapter 2: Solar cells fundamentals device

Figure 2.1 Solar spectral irradiance at air mass 0 and air mass 1.5 and the cutoff wavelength of GaAs and Si……..20
Figure 2.2 Schematic band diagrams for the photoluminescence processes in (a) A direct gap material, (b) An indirect gap material……...21
Figure 2.3 Structure and Band Diagram of a Photovoltaic Cell…….22
Figure 2.4 Simplest equivalent circuit, for an "ideal" solar cell; an external load resistance RL has also been drawn…….....23
Figure 2.5 (a) The I–V characteristic of an ideal solar cell and (b) the power produced by the cell. The power generated at the maximum power point is equal to the shaded rectangle in (a)…….24
Figure 2.6 The superposition principle for solar cells……..25
Figure 2.7 Universally used equivalent circuit for a solar cell…….26
Figure 2.8 Effect of (a) the series resistance Rs and of (b) the parallel resistance Rp, as given in the "universal" circuit of Fig. 2.13 on the J(V) characteristics of a solar cell. Values of (Rs)–1 and (Rp)–1 are given by the slopes of the J(V) characteristics, at the short-circuit point (V = 0) and at the open-circuit point (J = 0), respectively……26

Figure 2.9 Classification of photovoltaic cells…….27

Chapter 3: SCAPS-1D program

Figure 3.1: SCAPS the Action panel or main panel…….33
Figure 3.2 SCAPS working point……..…34
Figure 3.3 SCAPS spectrum and illumination……..35
Figure 3.4 SCAPS solar cell definition panel……..……..36
Figure 3.5 Parameters of the layer……...……..36
Figure 3.6 Batch set-up panel…….……...37
Figure 3.7 SCAPS energy band panel……...38

Chapter 4: Simulation and results

Figure 4.1 Schematic diagram of p-i-n GaAs solar cell…….……..42
Figure 4.2 Simulated structure of a GaAs p-i-n solar cell in SCAPS……..……..43
Figure 4.3 J-V characterisitic of p-i-n GaAs solar cell……..……44
Figure 4.4 Simulated photovoltaic parameters of GaAs solar cell as function of the acceptor concentration NA of p-layer…….……45
Figure 4.5 Simulated photovoltaic parameters of GaAs solar cell as function of the donor concentration ND of n-layer…….46
Figure 4.6 Simulated photovoltaic parameters of GaAs solar cell as function of thickness of the p-layer……...……47
Figure 4.7 Simulated photovoltaic parameters of GaAs solar cell as function of thickness of the i-layer…….…..48
Figure 4.8 Simulated photovoltaic parameters of GaAs solar cell as function of thickness of the n-layer……...……49
Figure 4.9 J-V characterisitic of optimized p-i-n GaAs solar cell……50

List of tables

Table 1.1 Portion periodic table related to semiconductors…….4
Table 4.1 Geometric and physical parameters set for simulation of the p-i-n GaAs solar cell...42
Table 4.2 Simulation and photovoltaic parameters of GaAs solar cells……43
Table 4.3 Simulation and photovoltaic parameters of optimized GaAs solar cells……..50

General Introduction

In recent decades, global electricity consumption has increased due to industrial, transport, and communication developments. Most electricity is still generated from non-renewable sources (coal, oil, gas, nuclear), which are expected to deplete in a few decades and contribute significantly to pollution. Thus, developing renewable energy sources, such as wind, oceanic currents, and solar energy, is crucial. Solar energy, in particular, is powerful, providing about 950 W/m² at ground level [1]. The solar energy received in just one week surpasses the total energy produced from global reserves of oil, coal, gas, and uranium, though converting solar radiation into electricity is often necessary. Gallium arsenide (GaAs) is a widely used III-V semiconductor in photovoltaic applications due to its high electron mobility, direct band gap, and effective growth mechanisms. GaAs single-junction devices can achieve efficiencies near 30%. These solar cells have been extensively studied and serve as a benchmark for thin-film solar cells due to their excellent electrical properties, heat resistance, and high performance [2] The following chapters explore semiconductor materials and their applications in solar cell technology. Chapter 1 discusses the electronic properties of semiconductors like silicon, germanium, and gallium arsenide (GaAs), emphasizing their crystal structures and energy bands. Chapter 2 covers solar cell fundamentals, detailing solar radiation principles and the photovoltaic effect while reviewing various solar cell types, including traditional silicon and new technologies, along with their efficiencies and applications. Chapter 3 introduces SCAPS-1D, a simulation program for modeling solar cells, guiding readers through its interface and simulation setup for different configurations. Chapter 4 focuses on optimizing GaAs solar cells, particularly the p-i-n structure, analyzing parameters like doping concentrations and layer thicknesses that influence efficiency. Overall, these chapters provide a thorough understanding of semiconductor materials and solar cell technology, highlighting optimization strategies for improved renewable energy solutions.

References

[1] E. Observ, “Baromètre du solaire photovoltaïque,” Systèmes Sol, vol. 160, pp. 69–83, 2004.

[2] GaAs Solar Cells https://sinovoltaics.com/learning-center/solar-cells/gaas-solar-cells/

CHAPTER 1:

Electronic properties of semiconductor materials

1.1 Introduction

Semiconductors play a crucial role in modern electronics, with silicon and germanium being among the most common. These materials, typically formed as single crystals, exhibit specific lattice structures that influence their electronic properties. Silicon and germanium, both belonging to the diamond lattice type, are elemental semiconductors, composed of a single species of atoms. Compound semiconductors like gallium arsenide (GaAs), which have a zinc blende lattice structure, are composed of different types of atoms and offer distinct advantages in various applications. This introduction provides a foundation for understanding the diverse characteristics and uses of semiconductor materials, particularly focusing on their crystal structures and energy bands.

1.2 Crystal structure

Most commonly used semiconductors are single crystals with diamond (with Si and Ge) or zinc blende (with GaAs and other compound semiconductors) lattice type as shown in Fig. 1.1.

Both lattices may be viewed as being composed of two interpenetrating face-centered cubic (fcc) sublattices that are displaced by one quarter of the distance along the diagonal of the cube. All atoms in the diamond lattice are identical, while the two fcc sublattices are built of different atoms in the case of III–V compounds such as GaAs. Each atom is surrounded by four close neighbors belonging to the other fcc sublattice [1].

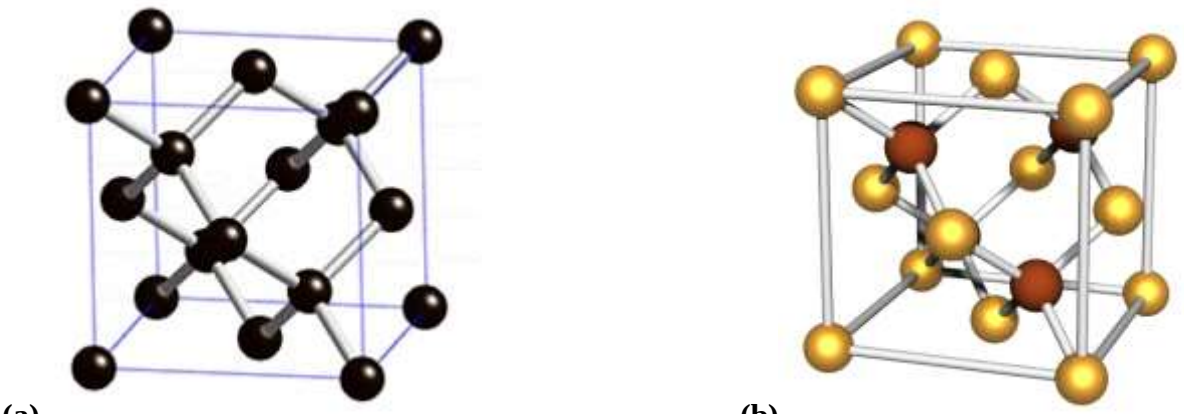

(a) **(b)**

Figure 1.1 (a) Diamond lattice, (b) Zinc blende lattice.

1.3 Element semiconductors

The study of semiconductor materials began in the early nineteenth century. Over the years many semiconductors have been investigated. Table 1.1 shows a portion of the periodic table related to semiconductors. The element semiconductors, those composed of single species of atoms, such as silicon (Si) and germanium (Ge), can be found in Column IV. In the early 1950s, germanium was the major semiconductor material. Since the early 1960s silicon has become a practical substitute and has now virtually supplanted germanium as a semiconductor material. The main reasons we now use silicon are that silicon devices exhibit better properties at room temperature, and high-quality silicon dioxide can be grown thermally. There are also economic considerations. Device-grade silicon costs much less than any other semiconductor material. Silicon in the form of silica and silicates comprises 25% of the Earth's crust, and silicon is second only to oxygen in abundance. Currently, silicon is one of the most studied elements in the periodic table, and silicon technology is by far the most advanced among all semiconductor technologies [2].

Period	Column II	III	IV	V	VI
2		B Boron	C Carbon	N Nitrogen	O Oxygen
3	Mg Magnesium	Al Aluminum	Si Silicon	P Phosphorus	S Sulfur
4	Zn Zinc	Ga Gallium	Ge Germanium	As Arsenic	Se Selenium
5	Cd Cadmium	In Indium	Sn Tin	Sb Antimony	Te Tellurium
6	Hg Mercury		Pb Lead		

Table 1.1 Portion periodic table related to semiconductors.

1.4 Energy Bands

Let's consider an isolated silicon atom (Si), where the energy levels of its electrons are discrete. When another identical atom is brought close to it, the discrete energy levels of its electrons split into two due to the reciprocal interaction between the two atoms. When N atoms

are brought close together, the energy levels split into N levels. These N levels are very close to each other, and if the value of N is large, as is the case in a crystal, these levels form a continuous energy band. The notion of atoms coming closer is given by the interatomic distance d.

Now, let's consider silicon atoms (Si) arranged at the nodes of a periodic lattice, but with a very large unit cell so that the atoms can be considered as isolated. The two most energetic levels are denoted by E_1 and E_2. If the atoms are brought closer together, the energy states split and form two continuous bands called the conduction band (CB) and the valence band (VB). Figure 1.2 shows the formation of these bands as a function of the interatomic distance.

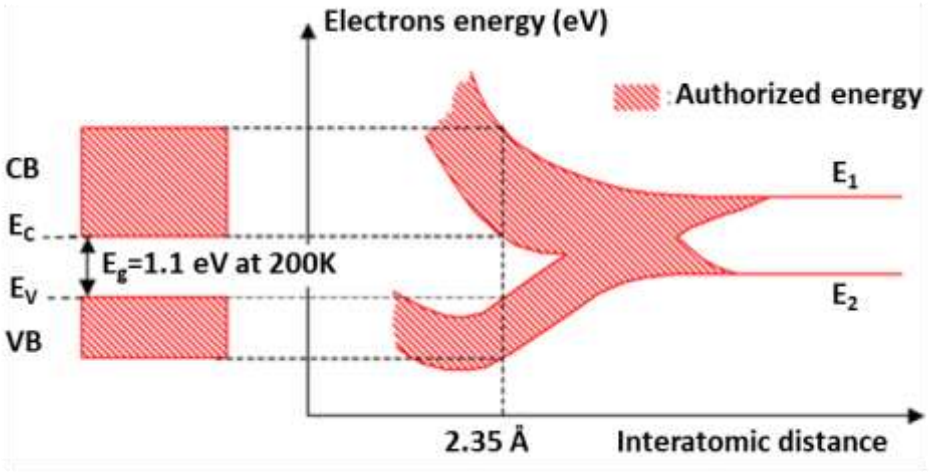

Figure 1.2 Formation des bandes d'énergie pour les électrons d'atomes de Si arrangés en mailles cristallines de type diamant.

For a silicon crystal (d_0 = 2.35 Å), it is observed that there are two continuous energy bands (the conduction band CB and the valence band VB), and these bands are separated by a forbidden band. This forbidden region is called the "gap," and its width, E_g, is characteristic of the material. Note that the energy at the bottom of the conduction band is denoted by E_C, and the energy at the top of the valence band is denoted by E_V, so we have the equation

$E_g = E_C - E_V$

At room temperature T = 300 K, E_g = 1.12 eV for silicon (Si) and Eg = 0.7 eV for germanium (Ge). In a semiconductor and at room temperature, some electrons move from the valence band to the conduction band [3].

1.5 Conduction in metals, semiconductors, and insulators

The enormous variation in electrical conductivity of metals, semiconductors, and insulators may be explained qualitatively in terms of their energy bands. Figure 1.3 shows the energy band diagrams of three classes of solids: metals, semiconductors, and insulators.

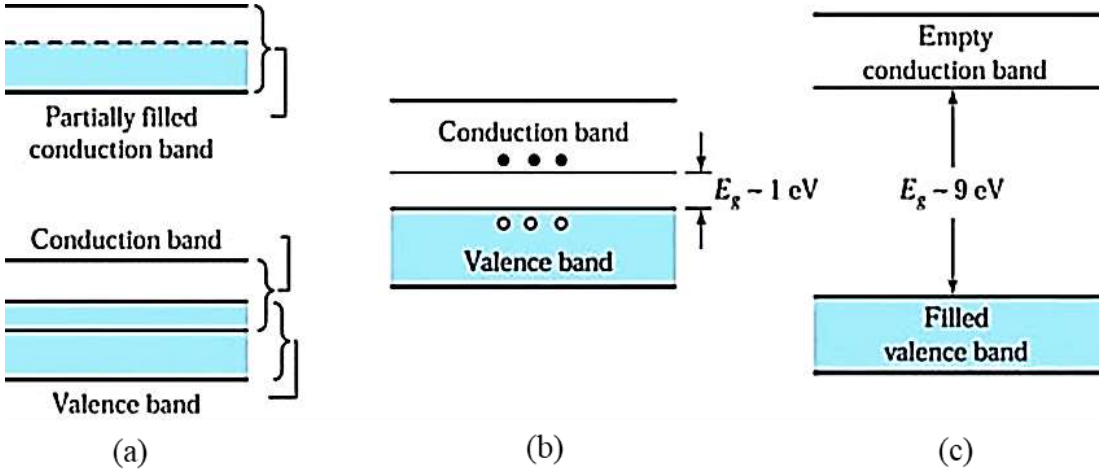

Figure 1.3 Schematic energy band representations of (a) a conductor with two possibilities (either the partially filled conduction band shown at the upper portion or the overlapping bands shown at the lower portion), (b) a semiconductor, (c) an insulator.

1.5.a Metals

The characteristics of a metal (also called a conductor) include a very low value of resistivity and a conduction band that either is partially filled (as in Cu) or overlaps the valence band (as in Zn or Pb) so that there is no bandgap, as shown in Fig. 1.3(a). As a consequence, the uppermost electrons in the partially filled band or electrons at the top of the valence band can move to the next higher available energy level when they gain kinetic energy (e.g., from an applied electric field). Electrons are free to move with only a small applied field in a metal because there are many unoccupied states close to the occupied energy states. Therefore, current conduction can readily occur in conductors.

1.5.b Semiconductors

Now, consider a material that has a much smaller energy gap, on the order of 1 eV (Fig. 1.3(b)). Such materials are called semiconductors. At $T = 0$ K, all electrons are in the valence band, and there are no electrons in the conduction band. Thus, semiconductors are poor

conductors at low temperatures. At room temperature and under normal atmospheres, values of E_g are 1.12 eV for Si and 1.42 eV for GaAs. At room temperature, appreciable numbers of electrons are thermally excited from the valence band to the conduction band. Since there are many empty states in the conduction band, a small applied potential can easily move these electrons, resulting in a moderate current.

1.5.c Insulators

In an insulator such as silicon dioxide (SiO_2), the valence electrons form strong bonds between neighboring atoms. Since these bonds are difficult to break, there are no free electrons to participate in current conduction at or near room temperature. As shown in the energy band diagram (Fig. 1.3(c)), insulators are characterized by a large bandgap. Note that electrons occupy all energy levels in the valence band and all energy levels in the conduction band are empty. Thermal energy or the energy of an applied electric field is insufficient to raise the uppermost electron in the valence band to the conduction band. Thus, although an insulator has many vacant states in the conduction band that can accept electrons, so few electrons actually occupy conduction band states that the overall contribution to electrical conductivity is very small, resulting in a very high resistivity. Therefore, silicon dioxide is an insulator; it cannot conduct current [2].

1.6 Intrinsic semiconductors

Intrinsic semiconductors contain no (in practice, very few) impurities compared with the number of thermally generated electrons and holes. For this condition we shall attempt to estimate the number of free charge carriers (electrons and holes) under equilibrium conditions. The occupation probability for an electronic state is given by the Fermi-Dirac function

$$f(E) = \frac{1}{1+\exp((E - E_F)/(k_B T))} \tag{1.1}$$

Where E_F, the Fermi energy, is the energy at which the occupation probability of a (possible) state is one half, k is the Boltzmann constant and T is the absolute temperature [1].

The density of free electrons n is obtained by integrating the carrier concentration (Fig. 1.4(d)) given by the product of the density of states N (Fig. 1.4(b)) and the occupation probability $F_n(E)$ (Fig. 1.4(c)) over the conduction band:

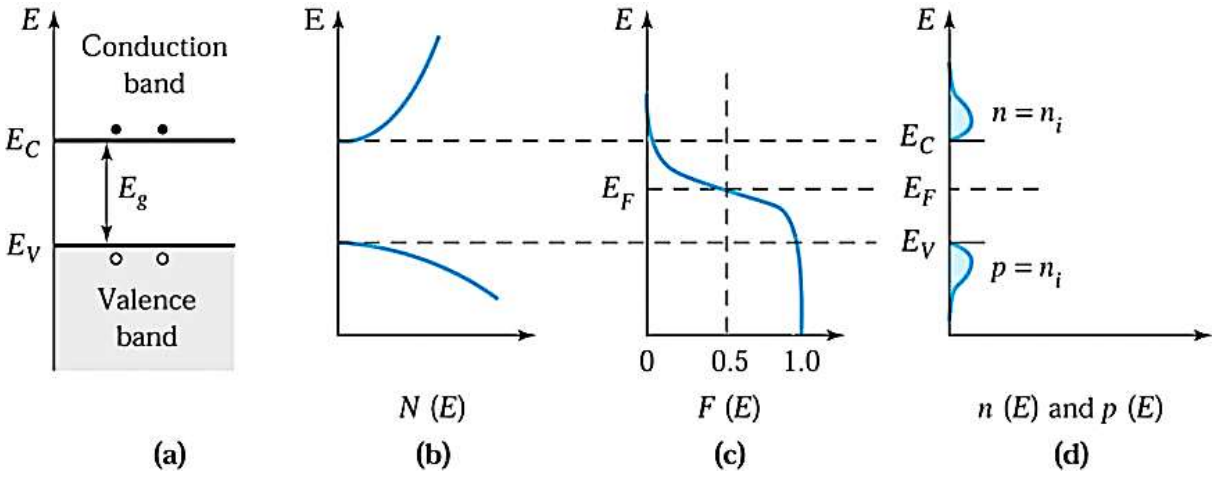

Figure 1.4 Intrinsic semiconductor: (a) Schematic band diagram, (b) Density of states, (c) Fermi distribution function, (d) Carrier concentration.

$$n = 2\left(\frac{2\pi m_n kT}{h^2}\right)^{\frac{3}{2}} e^{-\frac{E_C - E_F}{kT}} = N_C e^{-\frac{E_C - E_F}{kT}} \qquad (1.2(a))$$

Similarily for holes, we have:

$$p = 2\left(\frac{2\pi m_p kT}{h^2}\right)^{\frac{3}{2}} e^{-\frac{E_F - E_V}{kT}} = N_C e^{-\frac{E_F - E_V}{kT}} \qquad (1.2(b))$$

N_C and N_V are the effective densities of states in the conduction and valence bands respectively. The product of electron and hole concentration, given by $n.p = N_C N_V e^{-\frac{E_C - E_V}{kT}}$, depends on the band gap $E_G = E_C - E_V$ and is thus independent of the Fermi level E_F.

So far the value of the Fermi level E_F has not been specified and equations (1.1) to (1.2) will also be valid for extrinsic semiconductors (to be dealt with in the following chapter). The Fermi level for intrinsic semiconductors E_i can be found from the requirement that the numbers of electrons and holes are equal*:* $n = p = n_i$. One thus finds that:

$$n_i = \sqrt{N_C N_V}\, e^{-\frac{E_C - E_V}{2kT}} = \sqrt{N_C N_V}\, e^{-\frac{E_G}{2kT}} \qquad (1.3)$$

And

$$E_i = \frac{E_C + E_V}{2} + \frac{3kT}{4} \ln\left(\frac{m_p}{m_n}\right) \qquad (1.4)$$

where E_i is the Fermi level close to the middle of the band gap, the deviation being due to the unequal effective masses of electrons and holes.

Introducing the intrinsic carrier density n_i and the intrinsic level E_i, one may reformulate the more generally valid (1.2) in the useful form:

$$n = n_i e^{\frac{E_F - E_i}{kT}} \qquad p = n_i e^{\frac{E_i - E_F}{kT}} \tag{1.5}$$

1.7 Extrinsic semiconductors

Intrinsic semiconductors are rarely used in semiconductor devices since it is extremely difficult to obtain sufficient purity in the material. Moreover, in most cases one intentionally alters the property of the material by adding small fractions of specific impurities. This procedure, which can be performed either during crystal growth or later in selected regions of the crystal, is called doping. Depending on the type of added material, one obtains n-type semiconductors with an excess of electrons in the conduction band or p-type with additional holes in the valence band. We will look at extrinsic semiconductors through the simple bond representation and also through a band model.

Figure 1.5(a) shows a two-dimensional schematic bond representation of a silicon crystal with one silicon atom replaced by an arsenic atom with five valence electrons. Only four are used for the formation of covalent bonds with neighboring atoms, while the fifth is not bound to a specific atom but is free for conduction. It should be stressed that the crystal as a whole remains uncharged, since the charge of the free electron is compensated for by the excess charge of the arsenic nucleus bound in the crystal lattice.

If a silicon atom is replaced by an atom with only three valence electrons (Fig. 1.5(b)) one electron is missing in the covalent bonds and a hole is thus created. This hole may be filled by an electron from a neighboring atom, this being equivalent to a movement of the hole. The hole is free for conduction. (That the moving hole is more than a missing electron whose place is filled by a neighboring electron follows from quantum mechanical considerations and is experimentally verified in the Hall experiment) [1].

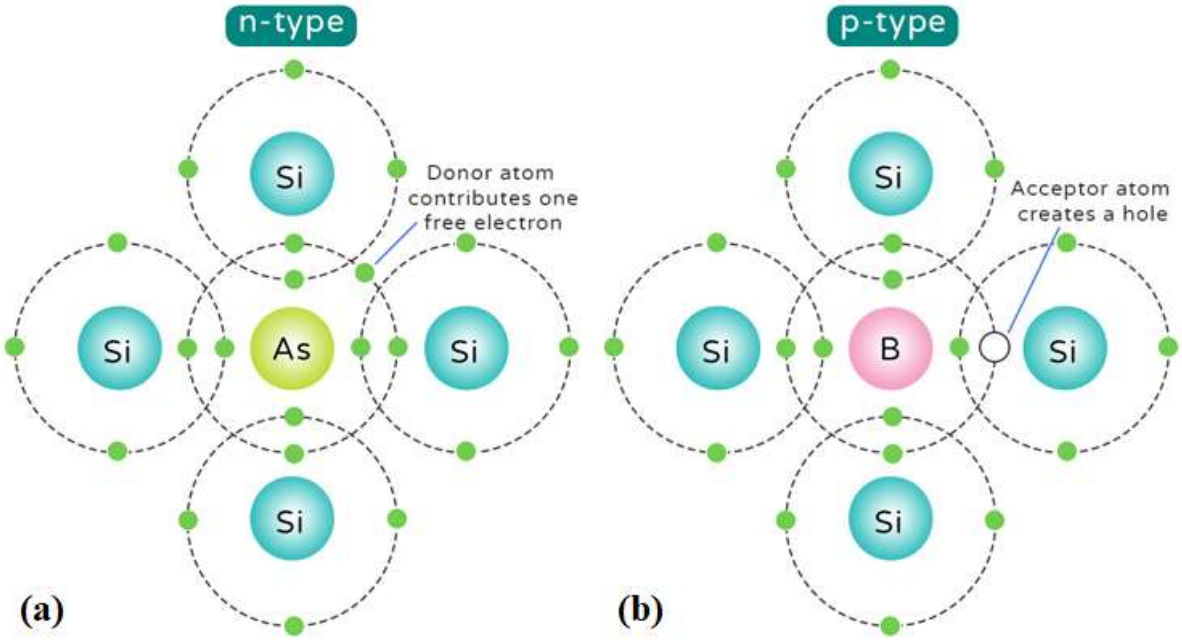

Figure 1.5 Schematic bond pictures for (a) n-type Si with donor (arsenic) and (b) p-type Si with acceptor (boron).

The replacement of a proper atom of the lattice by a different atom is accompanied by the creation of localized energy levels in the band gap. These energy levels may be of the donor (E_D) or acceptor (E_A) type. If donor levels E_D are close to the conduction band, as is the case for phosphorous ($E_C - E_D$ = 0.045 eV) or arsenic ($E_C - E_D$ = 0.054 eV) atoms in silicon, for instance, these states will be almost completely ionized at room temperature and the electrons will be transported to the conduction band (Fig. 1.6(a)). This is due to the many states with similar energy level nearby in the conduction band, with which the donor states have to share their electrons.

Equivalent considerations hold for acceptor-type states, e.g. boron in silicon ($E_A - E_V$ = 0.045 eV). These states will be filled almost completely and holes will be created in the valence band (Fig. 1.6(b)) [1].

The situation that the donor levels are almost completely ionized can be described by a movement of the Fermi level E_F from the intrinsic level E_i towards the conduction band.

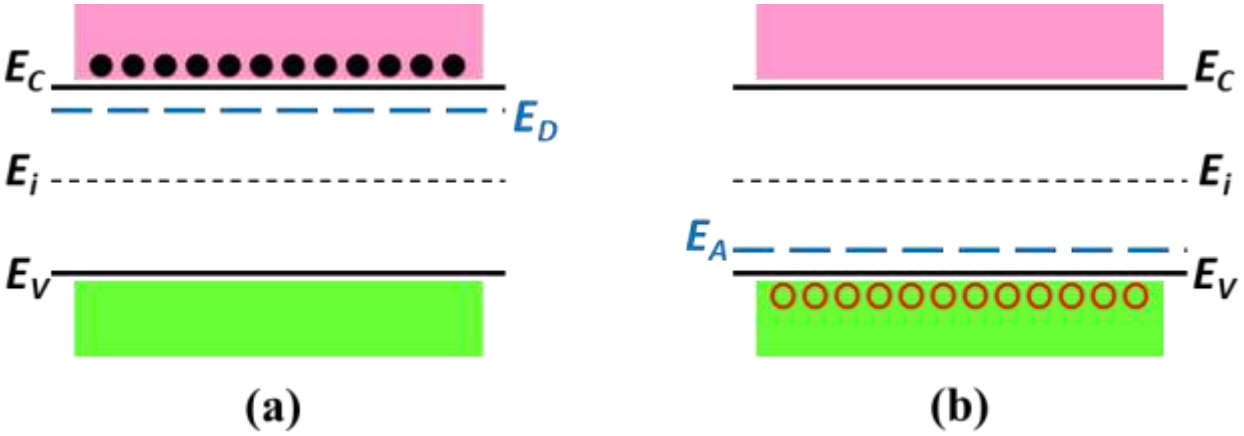

Figure 1.6 (a) Schematic energy band representation of extrinsic n-type, (b) p-type semiconductors.

By setting the electron concentration in the conduction band n equal to the donor concentration N_D, thus:

$$E_C - E_F = kT \ln \frac{N_C}{N_D} \tag{1.6}$$

Similarly, one obtains for p-type material and acceptor concentration N_A:

$$E_F - E_V = kT \ln \frac{N_V}{N_A} \tag{1.7}$$

A somewhat more complicated treatment is required for the simultaneous presence of donors and acceptors and for very high doping concentrations. It may also be mentioned in this context that the number of donor or acceptor states does not necessarily equal the number of corresponding impurity atoms, since in order to become electrically active doping atoms they have to be properly built into the crystal lattice [1].

The density of free electrons *n* is

$$n = n_i e \frac{E_F - E_i}{kT} \tag{1.8(a)}$$

The density of free holes *p* is

$$p = n_i e \frac{E_i - E_F}{kT} \tag{1.8(b)}$$

The increase of majority carriers (electrons in the case of n-type material) is accompanied by a decrease of minority carriers according to the mass-action law

$$n.p = n_i^2 \tag{1.9}$$

In agreement with (1.8) [1].

1.8 Currents in the Semiconductor

The currents in the semiconductor result from the movement of charge carriers, electrons, and holes, under the influence of different forces. The origin of these forces can be an electric field (conduction current) or a concentration gradient (diffusion current) [4].
The conduction current for each type of carrier (electrons, holes) is due to the electric field:

$$\overrightarrow{j_n} = en\mu_n \overrightarrow{E} \tag{1.9}$$

$$\overrightarrow{j_p} = ep\mu_p \overrightarrow{E} \tag{1.10}$$

The total current is then written as:

$$\overrightarrow{J_c} = e(n\mu_n + p\mu_p)\,\overrightarrow{E} = \sigma \overrightarrow{E} \tag{1.11}$$

With $\sigma = e(n\mu_n + p\mu_p)$ being the conductivity and $\mu_n(\mu_p)$ being the mobility of the electrons (holes).

When the free carriers are not uniformly distributed in the semiconductor, they undergo the diffusion process. The movement of charge carriers corresponds to diffusion currents:

$$\overrightarrow{j_{dn}} = eD_n \frac{dn}{dx} \tag{1.12}$$

$$\overrightarrow{j_{dp}} = -eD_p \frac{dp}{dx} \tag{1.13}$$

D_n and D_p are the diffusion constants of electrons and holes, respectively. The total diffusion current is then written as:

$$\overrightarrow{j_d} = eD_n \frac{dn}{dx} - eD_p \frac{dp}{dx} \tag{1.14}$$

Considering expressions (1.9), (1.10), and (1.12), (1.13), the resulting currents of electrons and holes are written as:

$$\overrightarrow{j_n} = e\mu_n n\overrightarrow{E} + eD_n \frac{dn}{dx} \quad (1.15.a)$$

$$\overrightarrow{j_p} = e\mu_p p\overrightarrow{E} - eD_p \frac{dp}{dx} \quad (1.15.b)$$

The diffusion constant D and the mobility μ of a type of carrier are related by the Einstein relation:

$$\frac{D_n}{\mu_n} = \frac{D_p}{\mu_p} = \frac{KT}{e} \quad (1.16)$$

1.9 Generation of Excess Carriers by Light

When a semiconductor is exposed to light excitation, electronic transitions are induced between the valence band and the conduction band, resulting in the creation of electron-hole pairs.

The energy required to create a pair is provided by a photon, and this energy is given by Planck's relation [4]:

$$E = h\nu = hc/\lambda \text{ (eV)} \quad (1.17)$$

such that h is Planck's constant = 4.14×10^{-15} eV.s, ν is the frequency s^{-1}; c is the speed of light = 3.10^{10} cm.s^{-1} and λ is the wavelength (cm).

Since all the energy of the photon is absorbed to ensure the electronic transition, it is required that: $h\nu > E_g$

To create an electron-hole pair, this condition can be expressed in terms of wavelength as:

$$\lambda(\mu m) < \frac{1.24}{E_g(eV)} \quad (1.18)$$

The calculation of the electron-hole pair generation rate $G(x)$ ($cm^{-3}s^{-1}$) is carried out as follows. Let ϕ_o represent the photon flux ($cm^{-2}s^{-1}$) incident on the illuminated surface of the material, and α (cm^{-1}) be the light absorption coefficient of the material. At depth x, this generation rate is:

$$G(x) = \alpha.\phi_o.e^{-\alpha.x} \tag{1.19}$$

1.10 Recombination of Excess Carriers

This process results in electrons from the conduction band falling into holes in the valence band. The semiconductor releases the energy as heat or emits light (photon). The following types of recombination can be distinguished:

a) Direct or band-to-band recombination: The electron falls directly into the hole in the valence band.

b) Indirect recombination: Involving deep levels in the bandgap, the electron first falls to this level and then into a hole in the valence band.

Recombination processes can also be classified based on how the energy is dissipated when the electron falls from the higher to the lower energy level:

a) Radiative recombination: The energy is released through the emission of photons.

b) Auger recombination: The energy is transferred to another electron or hole, which is then excited to a higher level in the conduction band or a lower level in the valence band.

c) Non-radiative recombination: The recovered energy is released in the form of phonons (heat) within the material [3].

1.11 Gallium Arsenide (GaAs): Properties, Uses

GaAs, a compound semiconductor classified as III–V, comprises gallium (Ga) from Group III and arsenic (As) from Group V of the periodic table. While Goldschmidt first synthesized GaAs in 1929, the electronic properties of III–V compounds as semiconductors were not reported until 1952 [5].

1.11.a Structure of GaAs

In a Gallium Arsenide (GaAs) wafer, each gallium atom is surrounded by arsenic atoms. The gallium atom, which has 3 valence electrons, and the arsenic atom, which has 5 valence electrons, share their electrons. This sharing allows both the gallium and arsenic atoms to

achieve a stable configuration with 8 valence electrons in their outer shells. It's important to note that a covalent bond forms between the gallium and arsenic atoms in the GaAs wafer. While these covalent bonds are strong, they can be broken if sufficient external energy is applied [6].

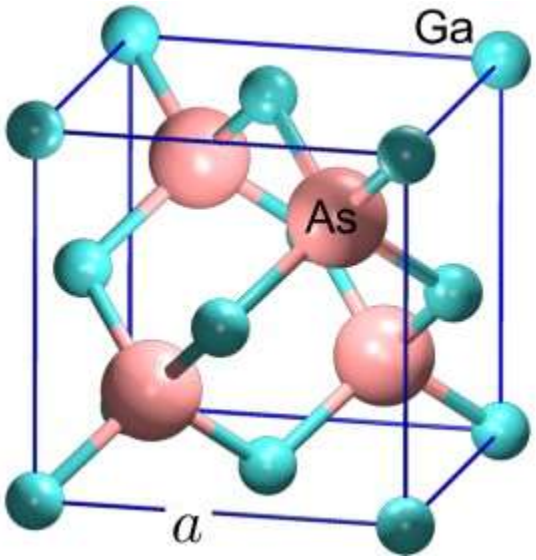

Figure 1.7 The structure of Gallium arsenide wafer.

1.11.b Properties of GaAs

Gallium arsenide (GaAs) outperforms silicon in several ways: it has higher electron mobility, supports frequencies up to 250 GHz in transistors, and is more resistant to high temperatures. GaAs also generates less noise in circuits and excels in light absorption and emission due to its direct bandgap. Its resistive nature and high dielectric constant make it ideal for integrated circuits, offering natural component isolation. These properties make GaAs suitable for satellites, mobile phones, and communication technology. GaAs wafers are modified through processes like ion implantation, doping, and etching for use in microelectronics [6].

1.11.c Use of GaAs

The main use of GaAs is found in:

- Computers.
- Photovoltaic cells.
- Optoelectronic communications.
- Laser diodes and infrared emission [6].

1.12 conclusion

Semiconductors are fundamental to modern electronics, with materials like silicon, germanium, and gallium arsenide each offering unique properties. Silicon's abundance and favorable characteristics have made it the primary choice for most applications, while gallium arsenide excels in high-speed and optoelectronic devices. Understanding the crystal structures, energy bands, and the effects of doping on semiconductor properties is crucial for developing advanced technologies. The interplay between these factors drives innovation in electronic devices, from transistors to photovoltaic cells.

Chapter 1 references

[1] G. Lutz, Semiconductor radiation detectors. Springer, 2007.

[2] S. M. Sze and M. K. Lee, “Semiconductor devices: phys-ics and technology. 3-rd edition.-New York, John Wiley and Sons, Inc,” 2012.

[3] Kateb mohamed Nadjib, Mokrani zakaria, "Conception et simulation électrique d’une cellule solaire en Si par le logiciel Tcad-Silvaco", mémoire de master, université Biskra, 2011.

[4] H. Mathieu, "Physique des semiconducteurs et des composants électroniques", 2ème Edition, Masson, 1990.

[5] Kayali S, Ponchak G, Shaw R. GaAs MMIC Reliability Assurance Guideline forSpace Applications. Jet Propulsion Laboratory, NASA, Tech. Rep. 1996 Dec 15.

[6] Gallium Arsenide (GaAs) Wafer: Structure, Properties, Uses. 21st Jul 2023. https://nanografi.com/blog/gallium-arsenide-gaas-wafer-structure-properties-uses/

CHAPTER 2:
Solar cells fundamentals device

2.1 introduction

This chapter provides a comprehensive overview of solar cell technology, beginning with the fundamentals of solar radiation and its impact on energy generation. It explores how the sun's energy is transferred to electrons in semiconductor materials, leading to electricity production through the photovoltaic effect. The chapter details the operation of solar cells, including the ideal and practical characteristics, and examines the different types of solar cells—ranging from traditional silicon-based to advanced emerging technologies. By the end, readers will gain a clear understanding of the principles, efficiencies, and applications of various solar cell technologies.

2.2 Solar radiation

The radiative energy output from the sun derives from a nuclear fusion reaction. Every second, about $6x10^{11}$ kg hydrogen is converted to helium, with a net mass loss of about $4x10^{3}$ kg. The mass loss is converted through the Einstein relation ($E = mc^2$) to $4x10^{20}$ J. This energy is emitted primarily as electromagnetic radiation in the ultraviolet to infrared region (0.2 to 3 μm). The total mass of the sun is now about $2x10^{30}$ kg, and a reasonably stable life with a nearly constant radiative energy output of over 10 billion (10^{10}) years is projected.

The intensity of solar radiation outside the earth's atmosphere, at the average distance of its orbit around the sun, is defined as the solar constant and has a value of 1367 W/m^2. Terrestrially, the sunlight is attenuated by clouds and by atmospheric scattering and absorption. The attenuation depends primarily on the length of the light's path through the atmosphere, or the mass of air through which it passes. This "*air mass*" is defined as $1/\cos\phi$, where ϕ is the angle between the vertical and the sun's position.

Figure 2.1 shows two curves related to solar spectral irradiance (power per unit area per unit wavelength). The upper curve, which represents the solar spectrum outside the Earth's atmosphere, is the air mass zero condition (AM0). The AM0 spectrum is relevant for satellite and space vehicle applications. Terrestrial solar cell performance is specified with reference to the air mass 1.5 (AM 1.5) spectrum. This spectrum represents the sunlight at the Earth's surface when the sun is at an angle of 48° from the vertical. At this angle the incident power is about 963 W/m² [1].

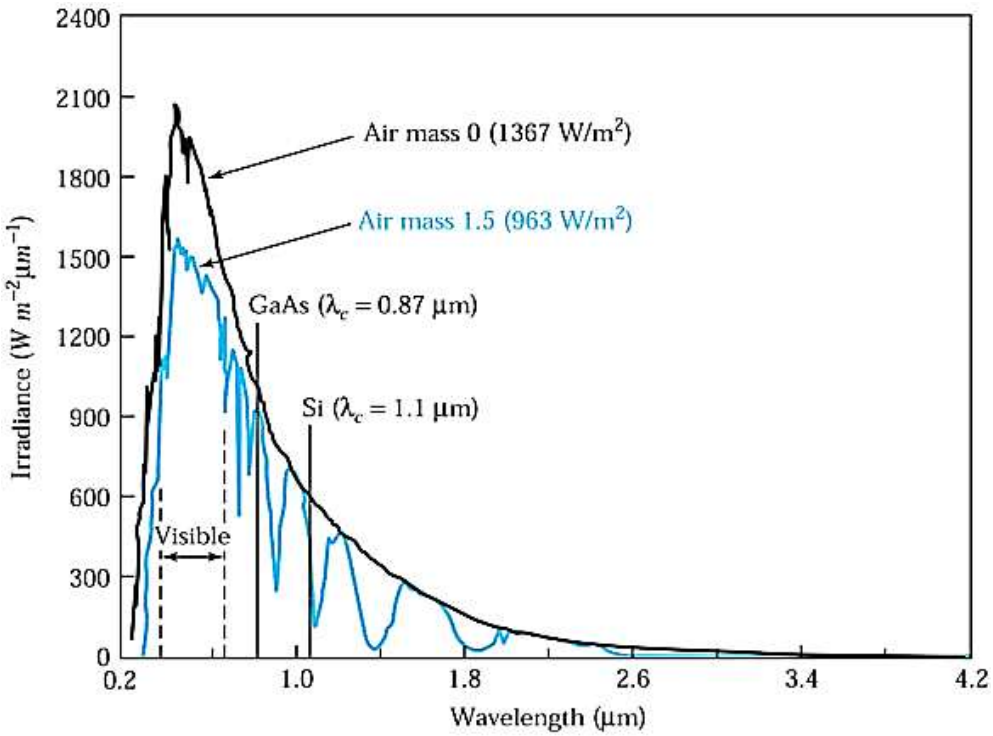

Figure 2.1 Solar spectral irradiance at air mass 0 and air mass 1.5 and the cutoff wavelength of GaAs and Si.

2.3 Transfer of energy from the photon to the electron

Each photon is characterized by a specific wavelength (λ) and an energy (Eph). Solar cells are sensitive to photons within a certain wavelength range, and only semiconductor materials possess the appropriate band structure required to generate usable electron-hole pairs from solar radiation. This process occurs when a photon is absorbed, allowing an electron in the valence band to transition to the conduction band, leaving behind a "hole" in the valence band, which acts as a pseudo-positive charge.

Figure 2.2 presents the different possible transitions according to the nature of the gap. When the minimum of the conduction band and the maximum of the valence band coincide in the K space, it is a direct gap. Inter-band transitions occur vertically, and are therefore radiative (Figure 2.2(a)). This illustrates the operation of III-V binary semiconductors, such as GaAs, which are widely used in optoelectronics. In the case of silicon (fig 2.2(b)), the gap is indirect: the electronic transitions between the extrema of the bands are oblique and non-radiative.

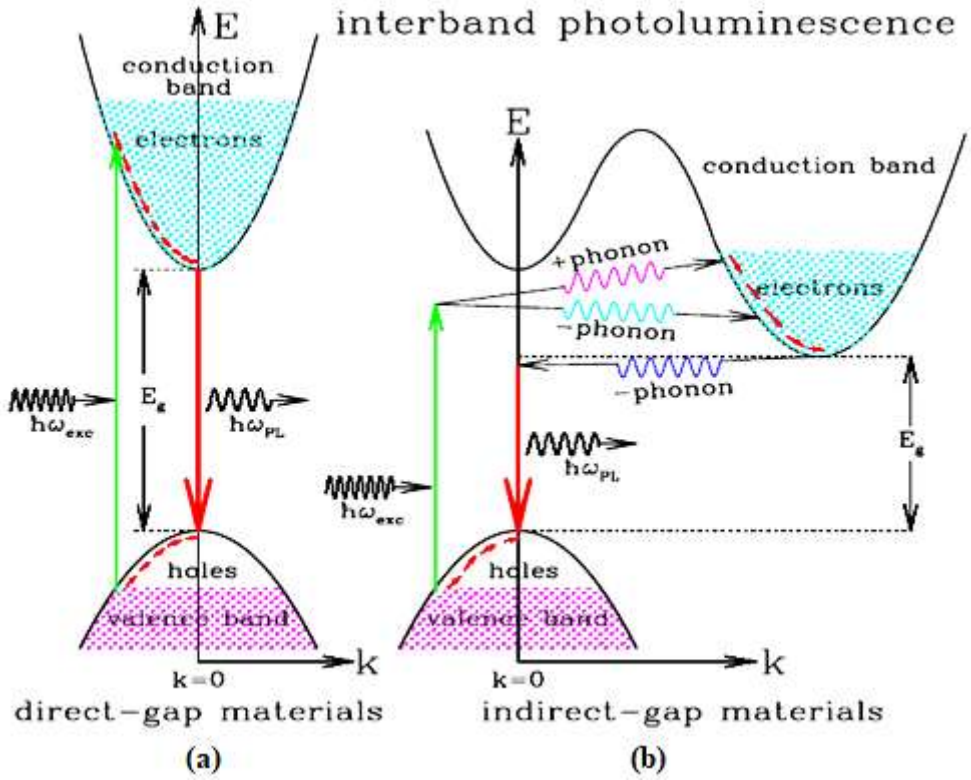

Figure 2.2 Schematic band diagrams for the photoluminescence processes in (a) A direct gap material, (b) An indirect gap material.

When a photon interacts with the semiconductor, it generates an electron-hole pair. To produce an electrical current, these photogenerated electron-hole pairs must be separated and collected by an external circuit before they can recombine within the material [2].

2.4 Principle of Operation of a Solar Cell

The photovoltaic effect used in solar cells allows the direct conversion of light energy from sunlight into electricity through the production and transport of positive and negative electric charges in a semiconductor material under the influence of light. This material consists of two parts: one with an excess of electrons and the other with a deficiency of electrons, referred to as n-type doped and p-type doped, respectively. When the n-type material is brought into contact with the p-type material, the excess electrons in the n-type material diffuse into the p-type material. As a result, the initially n-doped region becomes positively charged, and the initially p-doped region becomes negatively charged. This creates an electric field between them that tends to push the electrons back into the n-region and the holes into the p-region. This forms a PN junction. By adding metal contacts to the n and p regions, a diode is formed.

When the junction is exposed to light, photons with energy equal to or greater than the bandgap transfer their energy to atoms, each causing an electron to move from the valence band to the conduction band, leaving behind a hole capable of moving. This process generates an electron-hole pair. If a load is placed across the cell's terminals, the electrons from the n-region move toward the holes in the p-region through the external connection, creating a potential difference and causing an electric current to flow.

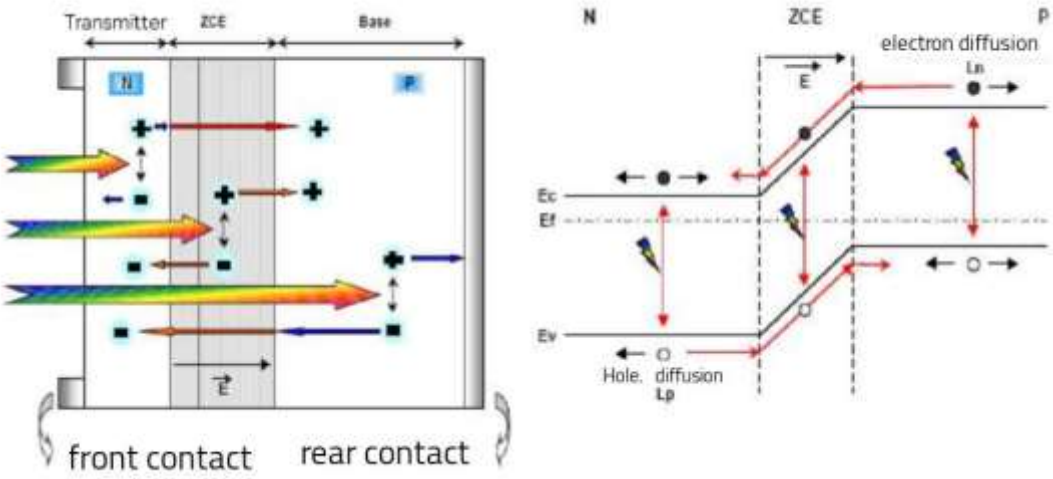

Figure 2.3 Structure and Band Diagram of a Photovoltaic Cell

The operating principle of a solar cell is illustrated in Figure 2.3. Incident photons generate charge carriers in the N and P regions, as well as in the space charge region. The behavior of these free carriers varies depending on where they are generated. In the electrically neutral P and N regions, the minority photocarriers diffuse. Those that reach the space charge region are driven by the electric field toward the region where they become majority carriers. These photocarriers contribute to the current through their diffusion, creating a diffusion photocurrent.

In the space charge region, electron-hole pairs created by photons are separated by the electric field, with electrons being driven toward the N-type region and holes toward the P-type region. These carriers give rise to a generation photocurrent. Both contributions combine to produce a resulting photocurrent (Iph), which adds to the reverse current of the diode [3].

2.5 Electrical characteristics

2.5.1 The ideal solar cell

An ideal solar cell can be represented by a current source connected in parallel with a rectifying diode, as shown in the equivalent circuit of Figure 2.4. The corresponding *I–V* characteristic is described by the Shockley solar cell equation:

$$I = I_{ph} - I_0\left(e^{\frac{qV}{k_BT}} - 1\right) \tag{2.1}$$

where k_B is the Boltzmann constant, T is the absolute temperature, q is the electron charge, and V is the voltage at the terminals of the cell. I_o is the diode saturation current. The photogenerated current I_{ph} is closely related to the photon flux incident on the cell, and its dependence on the wavelength of light is frequently discussed in terms of the quantum efficiency or spectral response.

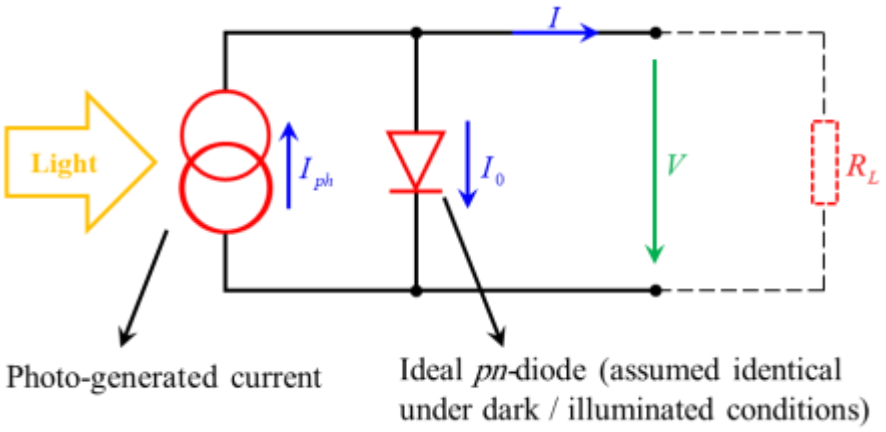

Figure 2.4 Simplest equivalent circuit, for an "ideal" solar cell; an external load resistance R_L has also been drawn.

Figure 2.5(a) shows the *I–V* characteristic (Equation (2.1)). In the ideal case, the short-circuit current I_{sc} is equal to the photogenerated current I_{ph}, and the open-circuit voltage V_{oc} is given by

$$V_{OC} = \frac{k_BT}{q}\ln\left(1 + \frac{I_{ph}}{I_0}\right) \tag{2.2}$$

The power $P=IV$ produced by the cell is shown in Figure 2.5(b). The cell generates the maximum power P_{max} at a voltage V_m and current I_m, and it is convenient to define the fill factor FF by:

$$FF = \frac{I_m V_m}{I_{sc} V_{oc}} = \frac{P_{\max}}{I_{sc} V_{oc}} \tag{2.3}$$

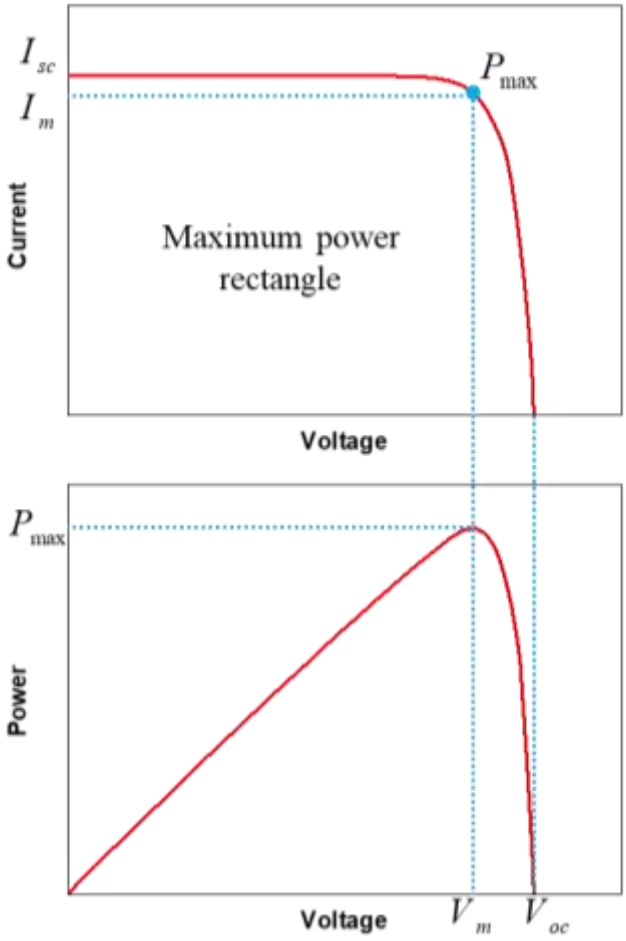

Figure 2.5 (a) The *I–V* characteristic of an ideal solar cell and (b) the power produced by the cell. The power generated at the maximum power point is equal to the shaded rectangle in (a).

The fill factor FF of a solar cell with the ideal characteristic (2.1) will be furnished by the subscript 0. It cannot be determined analytically but it can be shown that FF_o depends only on the ratio $v_{oc} = V_{oc} / k_B T$. FF_o is determined by the approximate expression.

$$FF_o = \frac{v_{oc} - \ln(v_{oc} + 0.72)}{v_{oc} + 1} \tag{2.4}$$

The efficiency η, of solar cells refers to the power conversion efficiency. It is defined as the ratio between the maximum power delivered by the cell and the incident light power P_{in}

$$\eta = \frac{P_m}{P_{in}} = \frac{FFV_{co}I_{cc}}{P_{in}} \tag{2.5}$$

P_{in} : the incident light power is equal to the solar power P_{solar} (P_{solar}= 100 mW/cm^2).

The *I–V* characteristics of an ideal solar cell complies with the *superposition principle:* the functional dependence (2.1) can be obtained from the corresponding characteristic of a diode in the dark by shifting the diode characteristic along the current axis by I_{ph} (Figure 2.6).

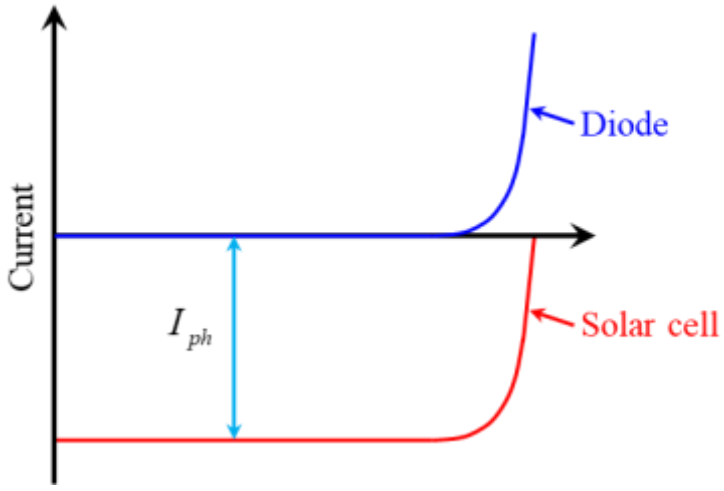

Figure 2.6 The superposition principle for solar cells.

2.5.2 Solar cell characteristics in practice

The *I–V* characteristic of a solar cell in practice usually differs to some extent from the ideal characteristic eq. (2.30). The solar cell (or circuit) may also contain series (R_s) and parallel (or shunt, R_p) resistances, leading to a characteristic of the form:

$$I = I_{ph} - I_0\left\{\exp\left(\frac{V + IR_s}{2k_BT}\right) - 1\right\} - \frac{V + IR_s}{R_p} \tag{2.6}$$

where the light-generated current I_{ph} may, in some instances, depend on the voltage. These features are shown in the equivalent circuit of Figure 2.7. The effect of the series and parallel resistances on the *I–V* characteristic of the solar cell is shown in Figures 2.8. The effect of the series resistance on the fill factor can be writing as [2, 4]:

$$FF = FF_o(1 - r_s) \tag{2.7}$$

where $r_s = R_s I_{sc}/V_{oc}$. An analogous expression exists also for the parallel resistance.

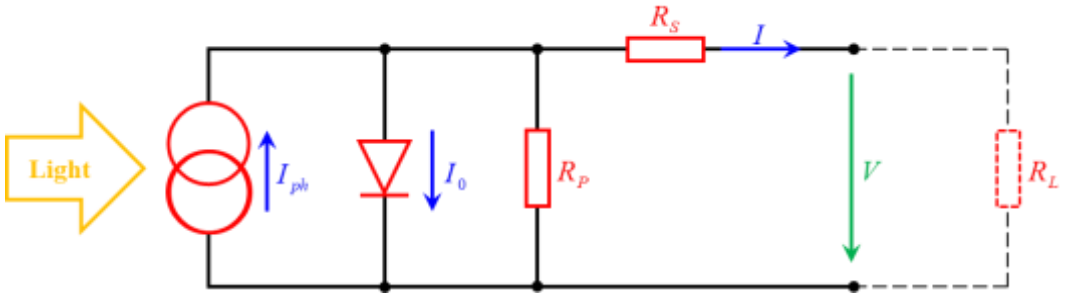

Figure 2.7 Universally used equivalent circuit for a solar cell.

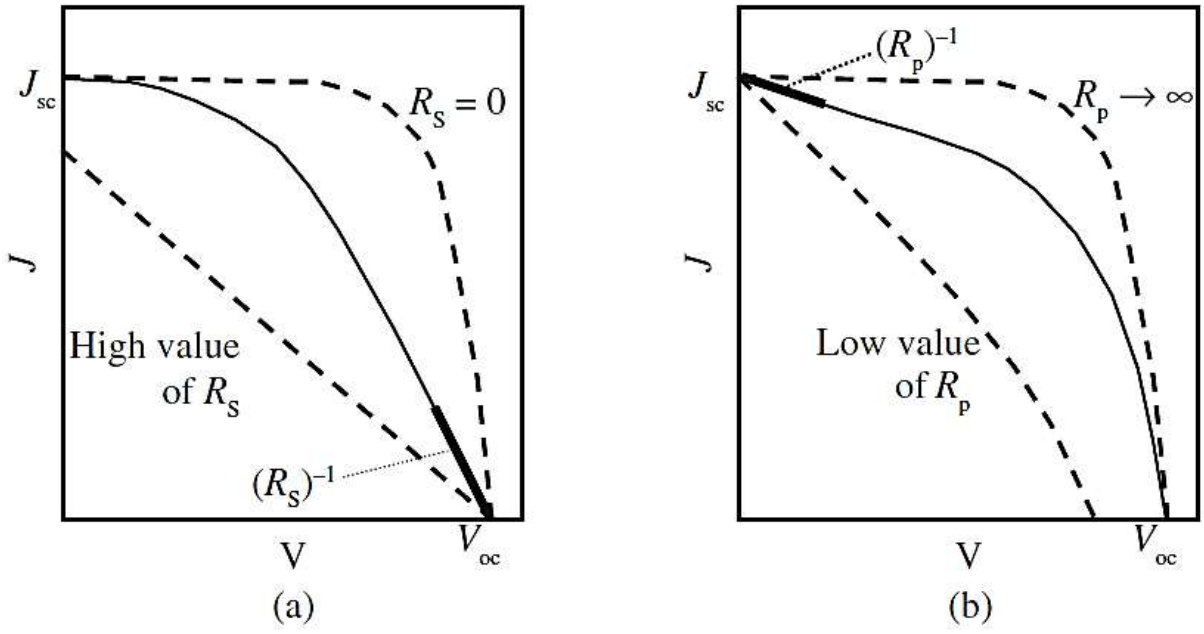

Figure 2.8 Effect of (a) the series resistance R_s and of (b) the parallel resistance R_p, as given in the "universal" circuit of Fig. 2.13 on the $J(V)$ characteristics of a solar cell. Values of $(R_s)^{-1}$ and $(R_p)^{-1}$ are given by the slopes of the $J(V)$ characteristics, at the short-circuit point ($V = 0$) and at the open-circuit point ($J = 0$), respectively.

2.6 Types of Solar Cells

Solar cells are classified into three generations: first, second, and third.

First-generation cells, also known as conventional, traditional, or wafer-based cells, are made from crystalline silicon. This is the most commercially dominant photovoltaic (PV) technology and includes materials such as polysilicon and monocrystalline silicon.

Second-generation cells are thin-film solar cells, which include materials like amorphous silicon, cadmium telluride (CdTe), and copper indium gallium selenide (CIGS). These are commonly used in utility-scale photovoltaic power stations, building-integrated photovoltaics, and small standalone power systems.

Third-generation cells represent various emerging thin-film technologies. Most are still in the research or development stage and have yet to see widespread commercial use. These cells often use organic materials, including organometallic compounds, as well as inorganic substances. Although their efficiency has traditionally been low, and the absorber materials tend to lack stability for long-term commercial applications, these technologies are the focus of significant research due to their potential to produce low-cost, high-efficiency solar cells.

Figure 2.15 shows various materials used to manufacture solar cells.

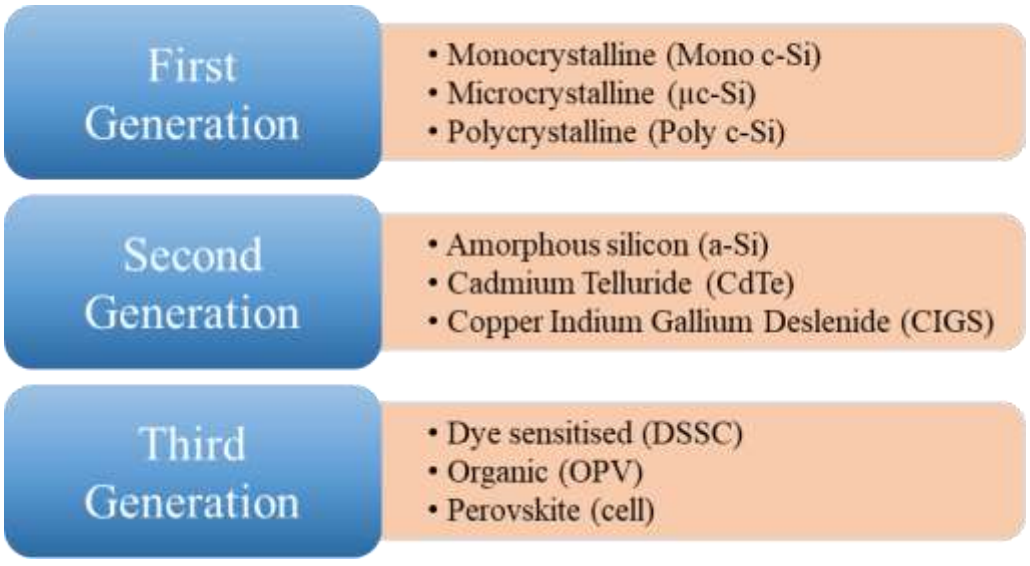

Figure 2.9 Classification of photovoltaic cells.

2.7 Conclusion

This chapter covered the fundamentals of solar cell technology, from how solar radiation is converted into electrical energy through the photovoltaic effect to the operational principles of different types of solar cells. It highlighted the distinction between ideal and practical performance, and reviewed various solar cell technologies—from traditional silicon-based to advanced emerging materials. Understanding these aspects is crucial for leveraging solar energy as a sustainable and efficient power source, paving the way for a cleaner, more renewable future.

Chapter 2 references

[1] S. M. Sze and M. K. Lee, “Semiconductor devices: phys-ics and technology. 3-rd edition.-New York, John Wiley and Sons, Inc,” 2012.

[2] Kateb Mohamed Nadjib, “Numerical simulation study of a-Si:H/µc-Si:H multijunction solar cell”, Phd thesis, Biskra University, 2022.

[3] H. Mathieu, "Physique des semiconducteurs et des composants électroniques", 6 ème Edition, Masson, 2009.

[4] T. Markvart, A. McEvoy, and L. Castaner, Practical handbook of photovoltaics: fundamentals and applications. Elsevier, 2003.

Chapter 3:

SCAPS-1D program

3.1 Introduction

In this chapter, we will explore SCAPS, a versatile solar cell simulation program. We'll start by understanding its development, key features, and how it can model various solar cell technologies. You'll learn how to navigate the SCAPS interface, set working points, define solar cell structures, and adjust parameters like temperature, voltage, and illumination. We will also cover how to simulate different measurements such as I-V, C-V, and quantum efficiency, along with the calculation methods SCAPS offers. Finally, you'll learn to analyze the simulated results and optimize solar cell designs using batch processing and curve fitting.

3.2 Fundamental equations in semiconductors

Semiconductors physics is an area very rich in modeling and mathematics problems. It consists of a fundamental set of equations that bring together electrostatic potential and load carriers in a very specific field of simulation. These equations, which are resolved via specific software for simulating semiconductor-based devices, are derived from Maxwell equations. They are mainly: Poisson's equation and continuity equations for both electrons and holes given by the following equations, which are used by SCAPS [1]:

$$\frac{\partial^2 \psi}{\partial x^2} + \frac{q}{\varepsilon}\left[p(x) - n(x) + N_D - N_A + \rho_p - \rho_n\right] = 0$$

$$\frac{1}{q}\frac{dJ_p}{dx} = G_{op}(x) - R(x)$$

$$\frac{1}{q}\frac{dJ_n}{dx} = -G_{op}(x) + R(x)$$

Ɛ: the dielectric constant, q: the electron charge, N_A: acceptor density, N_D: donor density

ψ: the electrostatic potential, p: hole concentration, n: electron concentration

ρ_p: hole distribution, ρ_n: electron distribution, J_p: current densities of hole

J_n: current densities of electron, G_{op}: the optical generation rate

R: the net recombination from direct and indirect recombination.

3.3 About SCAPS

SCAPS is a one dimensional solar cell simulation program developed at the department of Electronics and Information Systems (ELIS) of the University of Gent, Belgium. Several researchers have contributed to it is development: Alex Niemegeers, Marc Burgelman, Koen Decock, Johan Verschraegen, Stefaan Degrave.

The program is freely available to the PV research community (universities and research institutes). It runs on PC under Windows.

SCAPS is originally developed for cell structures of the CuInSe2 and the CdTe family. Several extensions however have improved its capabilities so that it is also applicable to crystalline solar cells (Si and GaAs family) and amorphous cells (a-Si and micromorphous Si).

An overview of its main features is given below [2]:

- Up to 7 semiconductor layers
- Almost all parameters can be graded (i.e. dependent on the ocal composition or on the depth in the cell): Eg, χ, ε, N_C, N_V, v_{thn}, v_{thp}, μ_n, μ_p, N_A, N_D, all traps (defects) N_t
- Recombination mechanisms: band-to-band (direct), Auger, SRH-type
- Defect levels: in bulk or at interface; their charge state and recombination is accounted for
- Defect levels, charge type: no charge (idealisation), monovalent (single donor, acceptor), divalent (double donor, double acceptor, amphoteric), multivalent (user defined)
- Defect levels, energetic distributions: single level, uniform, Gauss, tail, or combinations
- Defect levels, optical property: direct excitation with light possible (impurity photovoltaic effect, IPV)
- Defect levels, metastable transitions between defects
- Contacts: work function or flat-band; optical property (reflection of transmission filter) filter
- Tunneling: intra-band tunneling (within a conduction band or within a valence band); tunneling to and from interface states
- Generation: either from internal calculation or from user supplied *g(x)* file
- Illumination: a variety of standard and other spectra included (AM0, AM1.5D, AM1.5G, AM1.5Gedition2, monochromatic, white...)
- Illumination: from either the p-side or the n-side; spectrum cut-off and attenuation
- Working point for calculations: voltage, frequency, temperature
- The program calculates energy bands, concentrations and currents at a given working point, *J-V* characteristics, ac characteristics (*C* and *G* as function of *V* and/or *f*), spectral response (also with bias light or voltage)
- Batch calculations possible; presentation of results and settings as a function of batch parameters

- Loading and saving of all settings; start-up of SCAPS in a personalised configuration; a script language including a free user function
- Very intuitive user interface
- A script language facility to run SCAPS from a ‘script file’; all internal variables can be accessed and plotted via the script.
- A built-in curve fitting facility
- A panel for the interpretation of admittance measurements

3.4 SCAPS interface

SCAPS is a Windows-oriented program, developed with LabWindows/CVI of National Instruments. Scaps use the LW/CVI terminology of a ‘Panel’ (names used in other software’s are: a window, a page, a popup…). SCAPS opens with the ‘Action Panel’.

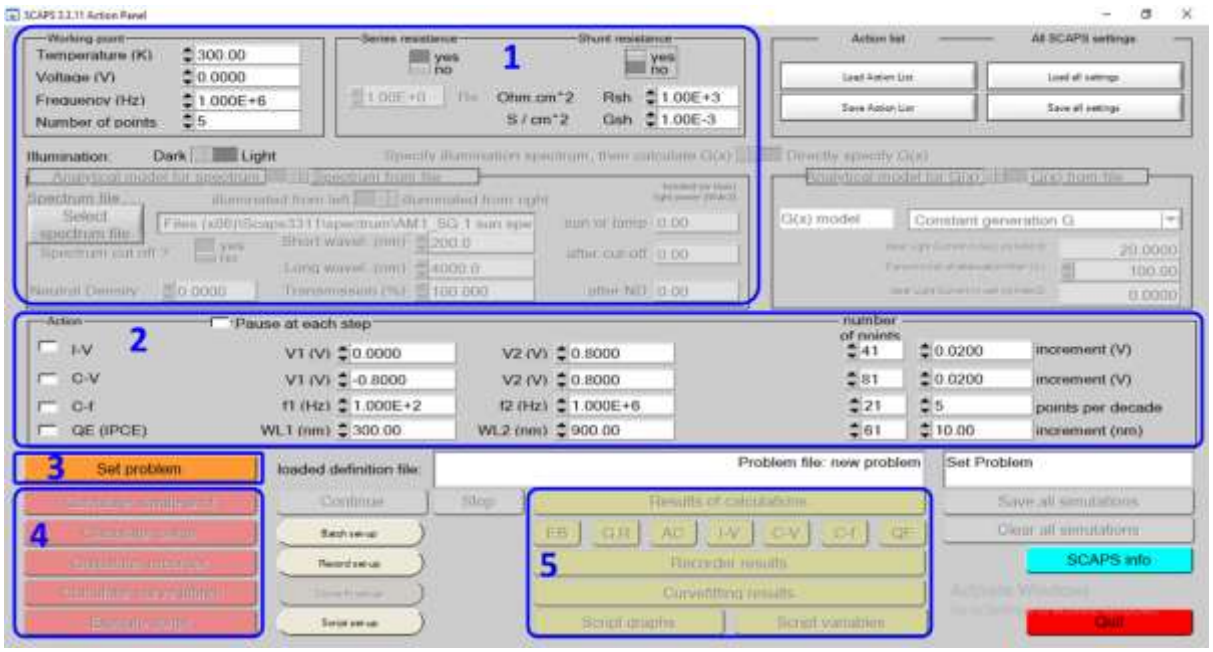

Figure 3.1: SCAPS the Action panel or main panel

The action panel consists of 5 parts

1. Working point
2. Indicate what you will calculate, i.e. which measurement you will simulate
3. Set problem (define the problem)
4. Start the calculation(s)
5. Display the simulated curves

3.5 Working point

The working point specifies the parameters which are not varied in a measurement simulation, and which are relevant to that measurement. Thus:

- The temperature *T*: relevant for all measurements. Note: in SCAPS, only N_C(T), N_V(T), the thermal velocities, the thermal voltage *kT* and all their derivatives are the only variables which have an explicit temperature dependence; you must input for each *T* the corresponding materials parameters yourself.
- The voltage *V*: is discarded in *I-V* and *C-V* simulation. It is the dc-bias voltage in *C-f* simulation and in *QE*(λ) simulation. SCAPS always starts at 0 V, and proceeds at the working point voltage in a number of steps that you also should specify.
- The frequency *f:* is discarded in *I-V*, *QE*(λ) and *C-f* simulation. It is the frequency at which the *C-V* measurement is simulated.
- The illumination: is used for all measurements. For the *QE*(λ) measurement, it determines the bias light conditions. The basis settings are: dark or light, choice of the illuminated side, choice of the spectrum. A one sun (= 1000 W/m^2) illumination with the 'air mass 1.5, global' spectrum is the default, but you have a large choice of monochromatic light and spectra for your specialized simulations. If you have an optical simulator at your disposal you can immediately load a generation profile as well instead of using a spectrum [2].

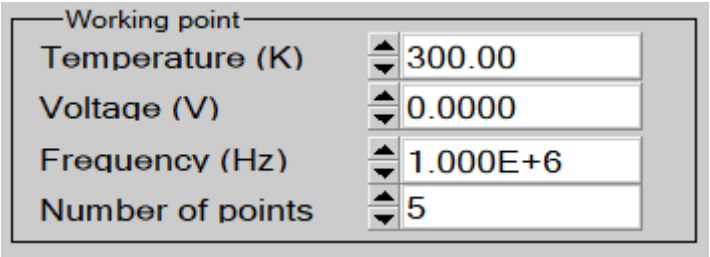

Figure 3.2 SCAPS working point

3.6 Spectrum and illumination:

Choose if you are simulating in dark or light, and select spectrum file you can find many files in SCAPS data base.

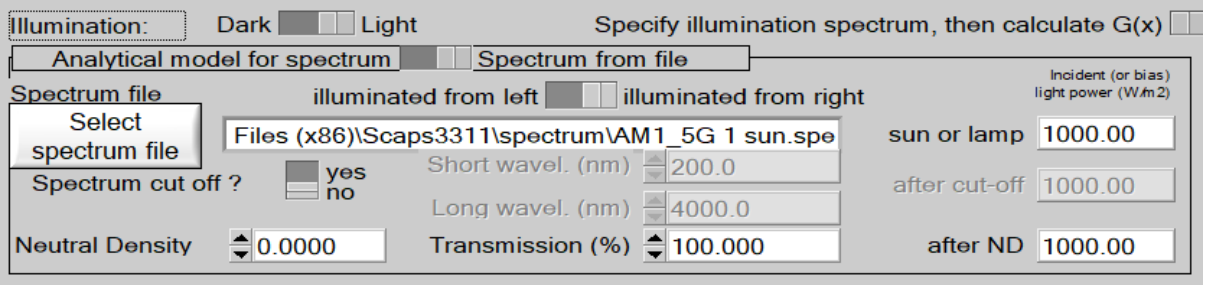

Figure 3.3 SCAPS spectrum and illumination

3.7 Select the measurement(s) to simulate

In the action-part of the Action Panel, you can select one or more of the following measurements to simulate: *I-V, C-V, C-f* and *QE*(λ). Adjust if necessary the start and end values of the argument, and the number of steps. Initially, do one simulation at a time, and use rather coarse steps: your computer and/or the SCAPS program might be less fast than you hope, or your problem could be really tough... A hint: in a *C-V* simulation, the *I-V* curve is calculated as well; no need then to specify it separately [2].

3.8 Define the problem

When clicking the 'Set Problem'-button on the action panel, the 'Solar cell definition'-panel is displayed. This panel allows to create/edit solar cell structures and to save those to or load from definition files. These definition files are standard ASCII-files with extension '*.def' which can be read with e.g. notepad. Even though the format of these files seems self-explaining it is however strongly advised not to alter them manually. You can design your solar cell and change different layers by clicking on add layer and modify properties such us thickness, band gap [2].

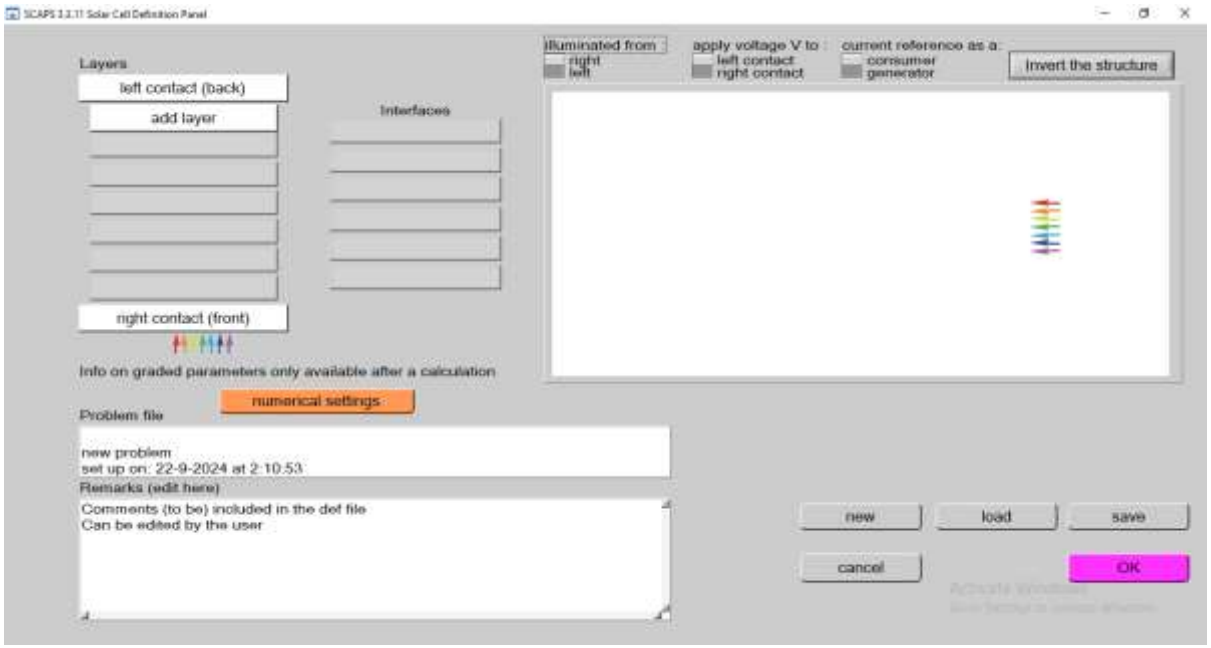

Figure 3.4 SCAPS solar cell definition panel

3.9 Change parameters:

By clicking on a layer, you can alter its thickness and band gap, among other factors.

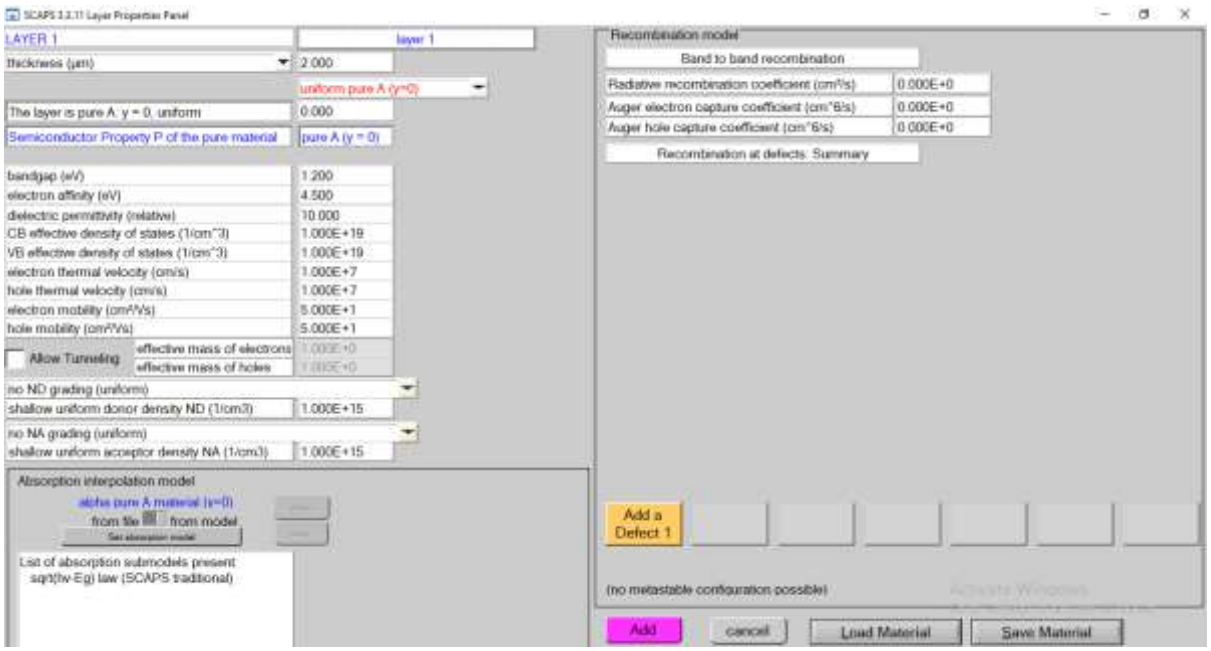

Figure 3.5 Parameters of the layer

3.10 Start the calculation(s)

We have 3 different types of calculation single shot, batch and recorder:

- **Single shot calculation:** when clicking on the button (calculate: single shot) the calculations start. At the bottom of the Panel, you see a status line, e.g. "iv from 0.000 to 0.800 Volt: $V = 0.550$ Volt", showing you how the simulation proceeds. Meanwhile, SCAPS stands you a free movie how the conduction and valence bands, the Fermi levels and the whole caboodle are evolving. When you see the hated divergence message, you're entitled to get into a bad mood, but don't exaggerate. Anyway, you did not lose the *I-V* points already calculated.
- **Batch calculation:** When you want to explore the influence of one or a few parameters to the solar cell characteristics, you can take profit of the batch option. When you click Batch set-up, a panel opens where you can choose which parameter to vary, over which range, and in which mode (Lin, Log or custom). You can also define more than one parameter, and vary all of them (in a nested way or 'simultaneous'), but be modest to start. A batch calculation is launched when calculate: batch is clicked [2].

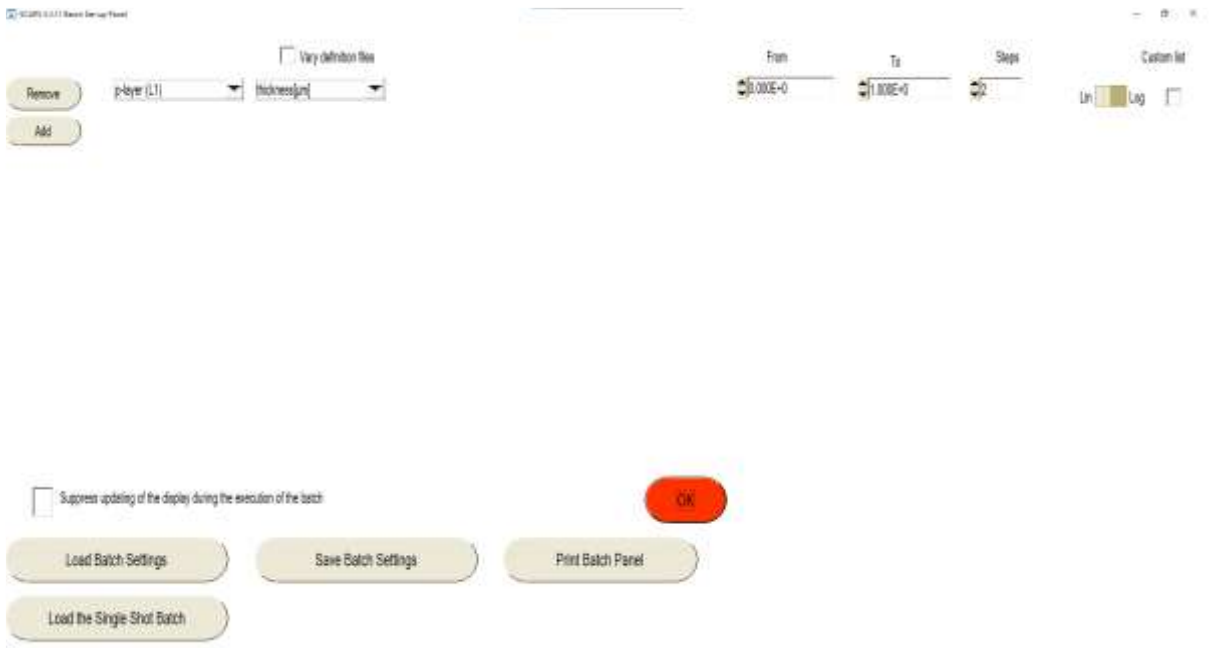

Figure 3.6 Batch set-up panel

3.11 Display the simulated curves:

After the calculation(s), SCAPS switches to the Energy band panel (or the AC-band panel). You can now look at your ease to the band diagrams; carrier densities, current densities, at the

last bias point calculated (stop your calculations earlier, or use the pause button on the Action Panel if you want to look at an intermediate state at ease). You can output the results (buttons print, save graphs, show (then the numbers are shown on screen; cut & paste to e.g. Excel is possible), or save (then the numbers are saved to a file). You can switch to one of the specialized output Panels (if you have already simulated at least one corresponding measurement). We only show the example of the IV Panel [2].

Figure 3.7 SCAPS energy band panel

3.12 Conclusion

In conclusion, SCAPS is a powerful and flexible tool for simulating and analyzing solar cell performance. Throughout this chapter, we explored its features, interface, and capabilities in modeling various cell types and measurements. By mastering SCAPS, researchers can gain valuable insights into solar cell behavior, optimize designs, and better understand key parameters affecting efficiency and performance. This makes SCAPS an essential resource for advancing photovoltaic research and development.

Chapter 3 references

[1] KHELFAOUI Hala, “Simulation of thin film solar cells using the SCAPS-1D program”, mémoire de master, universite Kasdi Merbah Ouargla, 2023.

[2] Burgelman M, Decock K, Niemegeers A, et al. SCAPS manual most recent. Version 2021.

Chapter 4: Simulation and results

4.1 Introduction

In this chapter, we will explore the design, simulation, and optimization of GaAs (gallium arsenide) solar cells. We begin with an introduction to the GaAs solar cell, specifically focusing on the p-i-n structure, where an intrinsic (i-GaAs) layer is sandwiched between p-type and n-type GaAs layers. Next, we'll dive into the optimization of key parameters, including doping concentrations and layer thicknesses, to enhance the cell's efficiency. By adjusting the acceptor concentration in the p-layer and the donor concentration in the n-layer, we can see small but important increases in efficiency. Similarly, optimizing the thickness of each layer allows us to maximize the solar cell's efficiency, with simulations showing that a GaAs solar cell can reach efficiencies up to 30%. By the end of this chapter, we will have a comprehensive understanding of how to design and optimize GaAs solar cells for maximum performance.

4.2 GaAs solar cell

III-V compound solar cells, such as GaAs (gallium arsenide) solar cells, offer several advantages over traditional crystalline silicon (Si) solar cells. These advantages include high efficiency potential, the ability to produce thin-film versions, a favorable temperature coefficient, radiation resistance, and suitability for multi-junction applications. III-V compound solar cells have found key applications in space and concentrator solar cells and serve as crucial sub-cells in multi-junction solar cell designs. Extensive research and development have resulted in impressive efficiency records for single-junction III-V compound solar cells, with GaAs solar cells achieving an efficiency of 29.1% [1, 2; 3]

4.3 Device structure of p-i-n GaAs solar cell and simulation parameters

Figure 4.2 presents the structure of a p-i-n GaAs solar cell, with the physical parameters used in the numerical simulation listed in Table 1. This structure features an intrinsic GaAs (i-GaAs) region sandwiched between n-GaAs and p-GaAs layers. The p-i-n configuration creates an electric field between the p and n regions, which efficiently separates electron-hole pairs and minimizes recombination. When light is absorbed, electrons are excited from the valence band to the conduction band, leaving behind holes in the valence band. These charge carriers move through the material, contributing to the generation of photocurrent.

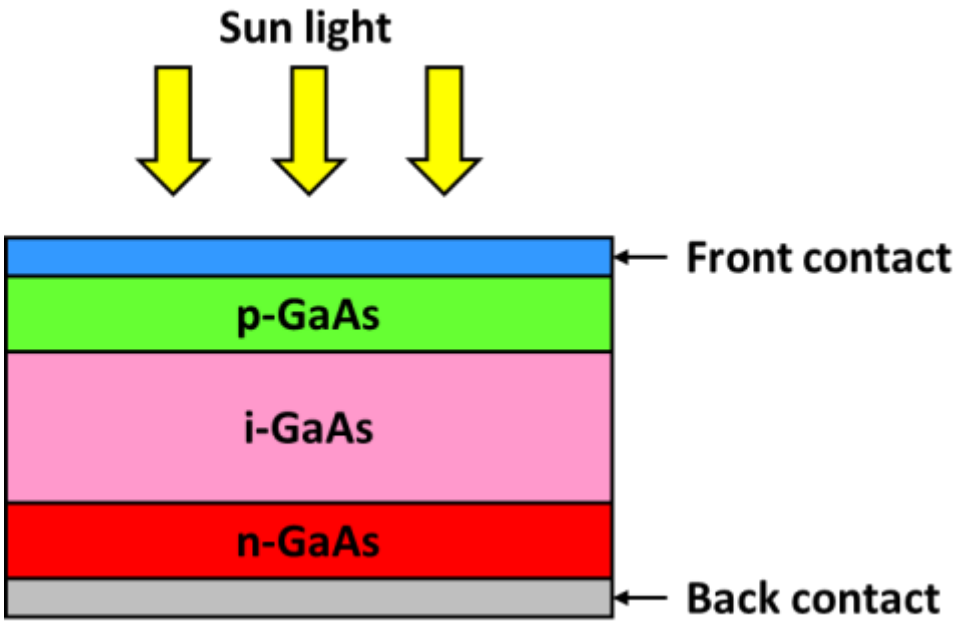

Figure 4.1 Schematic diagram of p-i-n GaAs solar cell.

Parameters	***n-GaAs***	***i- GaAs***	***p-GaAs***
Thickness (μm)	300	100	200
bandgap (eV)	1.420	1.420	1.420
electron affinity (eV)	4.070	4.070	4.070
dielectric permittivity (relative)	13.200	13.200	13.200
CB effective density of states $(1/cm^3)$	4.7×10^{17}	4.7×10^{17}	4.7×10^{17}
VB effective density of states $(1/cm^3)$	7×10^{18}	7×10^{18}	7×10^{18}
electron thermal velocity (cm/s)	2.1×10^{7}	2.1×10^{7}	2.1×10^{7}
hole thermal velocity (cm/s)	2.1×10^{7}	2.1×10^{7}	2.1×10^{7}
electron mobility (cm^2/Vs)	8.5×10^{3}	8.5×10^{3}	8.5×10^{3}
hole mobility (cm^2/Vs)	4×10^{2}	4×10^{2}	4×10^{2}
shallow uniform donor density $N_D(1/cm^3)$	1×10^{18}	2.1×10^{6}	0
shallow uniform acceptor density $N_A(1/cm^3)$	0	2.1×10^{6}	1×10^{11}

Table 4.1 Geometric and physical parameters set for simulation of the p-i-n GaAs solar cell [4; 5, 6, 7].

4.4 solar cell performance

The first simulation step consists of the simulation of GaAs based p-i-n solar cell. The parameter values adopted in the simulation are given in Tables 4.1

Simulation studies are carried out using an GaAs p–i–n structure consisting of frontcontact/p-GaAs (300 nm)/i-GaAs (100 nm)/n-GaAs (200 nm)/backcontact which is shown in figure 4.2.

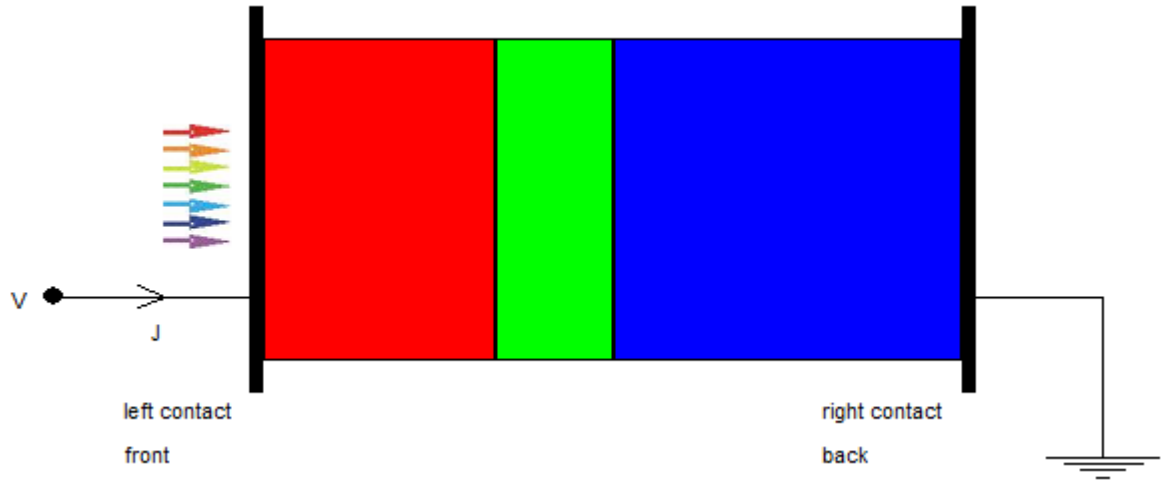

Figure 4.2 Simulated structure of a GaAs p-i-n solar cell in SCAPS.

The J–V characteristic simulated for GaAs solar cell is presented in figure 4.3. Table 4.2 shows the photo electrical parameters of GaAs solar cell extracted from the corresponding J–V characteristic.

Table 4.2 Simulation and photovoltaic parameters of GaAs solar cells.

	J_{sc}(mA/cm^2)	V_{oc}(V)	*FF* (%)	η (%)
p-i-n GaAs cell simulation	28.72	1.03	88.36	26.17

The electrical characteristics of the GaAs solar cell obtained through simulation are, respectively, *Jsc*=28.72 mA/cm^2, *Voc*=1.03 V, *FF*=88.36 %, η=26.17 % These results obtained from the simulation are very reasonable and even good results, and they belong to the known and applicable field in the field of solar cells based on GaAs.

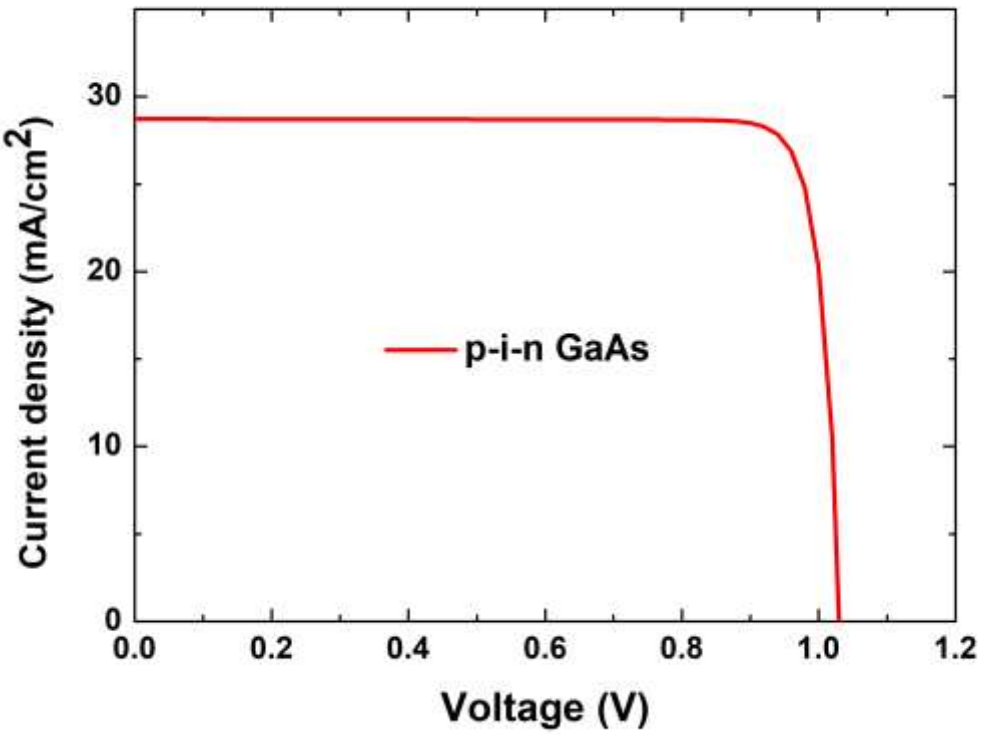

Figure 4.3 $J-V$ characterisitic of p-i-n GaAs solar cell.

4.5 Optimization of GaAs solar cell performance

In a second stage, we improved the performance of the solar cell by:

- Optimization of acceptor and donor concentrations of p layer and n layer respectively.
- Optimization of thicknesses of solar cell p, i and n layers.

4.5.a Optimization of acceptor concentrations of GaAs solar cell p-layer

Many simulations are executed with the variations of the acceptor concentration N_A from 10^{18} cm^{-3} to 10^{19} cm^{-3} of p-layer (Fig. 4.4). However, with the increasing of N_A, (*Jsc*,*Voc* and *FF* remains constant) The efficiency η increased slightly from 26.17 % to 26.67 %. The results indicate that the dopant concentration N_A enhances the efficiency. The p-layer concentration of 10^{19} cm^{-3} may be considered an optimized value.

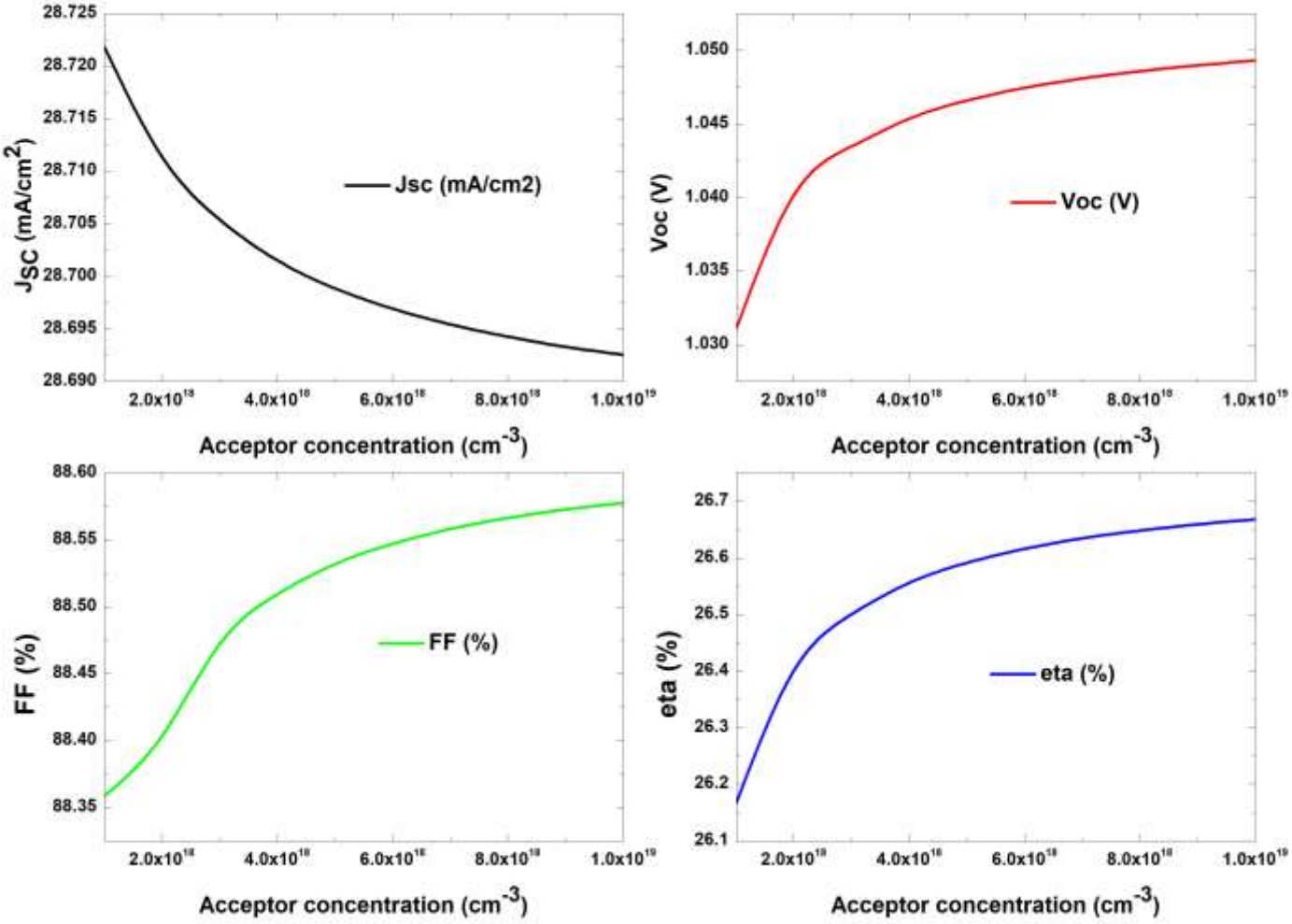

Figure 4.4 Simulated photovoltaic parameters of GaAs solar cell as function of the acceptor concentration N_A of p-layer.

4.5.b Optimization of donor concentrations of solar cell n-layer

The simulations are executed with the variations of the donor concentration N_D from 10^{18} cm^{-3} to 10^{19} cm^{-3} of n-layer (Fig. 4.5). However, with the increasing of N_D , *Jsc* remains constant, ,*Voc* increased slightly from 1.05 V to 1.1 V, *FF* increased slightly from 88.57% to 88.97% and The efficiency η increased from 26.67 % to 27.82 %. The results indicate that the dopant concentration N_D enhances the efficiency. The n-layer concentration of 10^{19} cm^{-3} considered an optimized value.

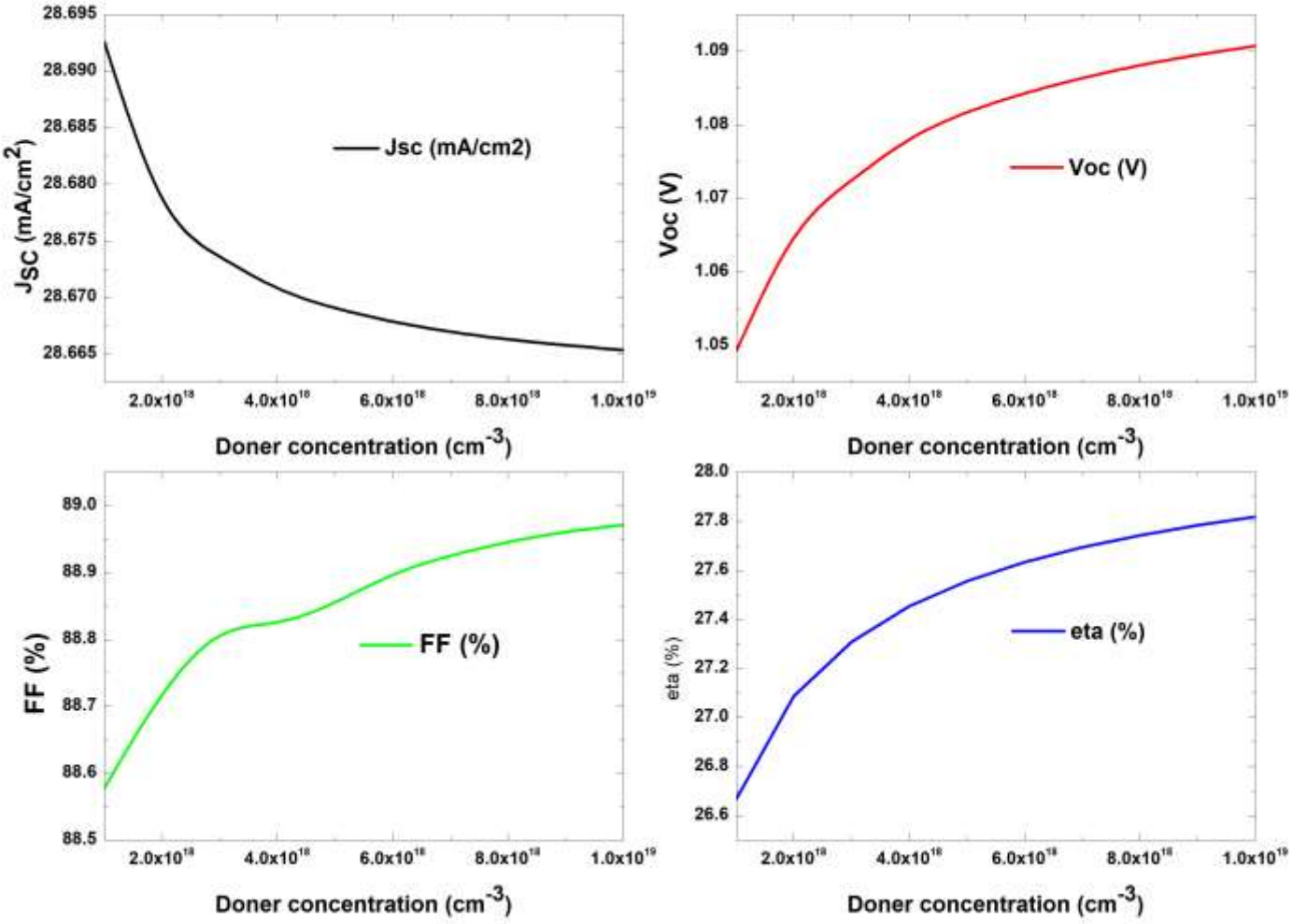

Figure 4.5 Simulated photovoltaic parameters of GaAs solar cell as function of the donor concentration N_D of n-layer.

4.5.c Optimization of thicknesses of solar cell p-layer

Once we obtained optimal dopant concentrations by simulation, we performed optimizing the thickness on the photoelectrical parameters of GaAs solar cell. This study is carried out by taking constant dopant concentrations of n- and p- layers as 10^{19} cm^{-3} and 10^{19} cm^{-3}, respectively. In view of this, we have also examined the behaviours of J_{sc}, V_{oc}, FF and η as a function of thickness of layers. As shown in Fig.4.6, with increasing p layer thickness from 0.05 µm to 1.5 µm, J_{sc} has a maximum value of 30.06 $mA.cm^{-2}$ at p layer thickness of 0.8 µm, V_{oc} and FF show a very small variation. η has a maximum value of 29.22 % at p layer thickness of 0.8 µm. The results indicate that the p layer thickness of 0.8 µm enhances the efficiency.

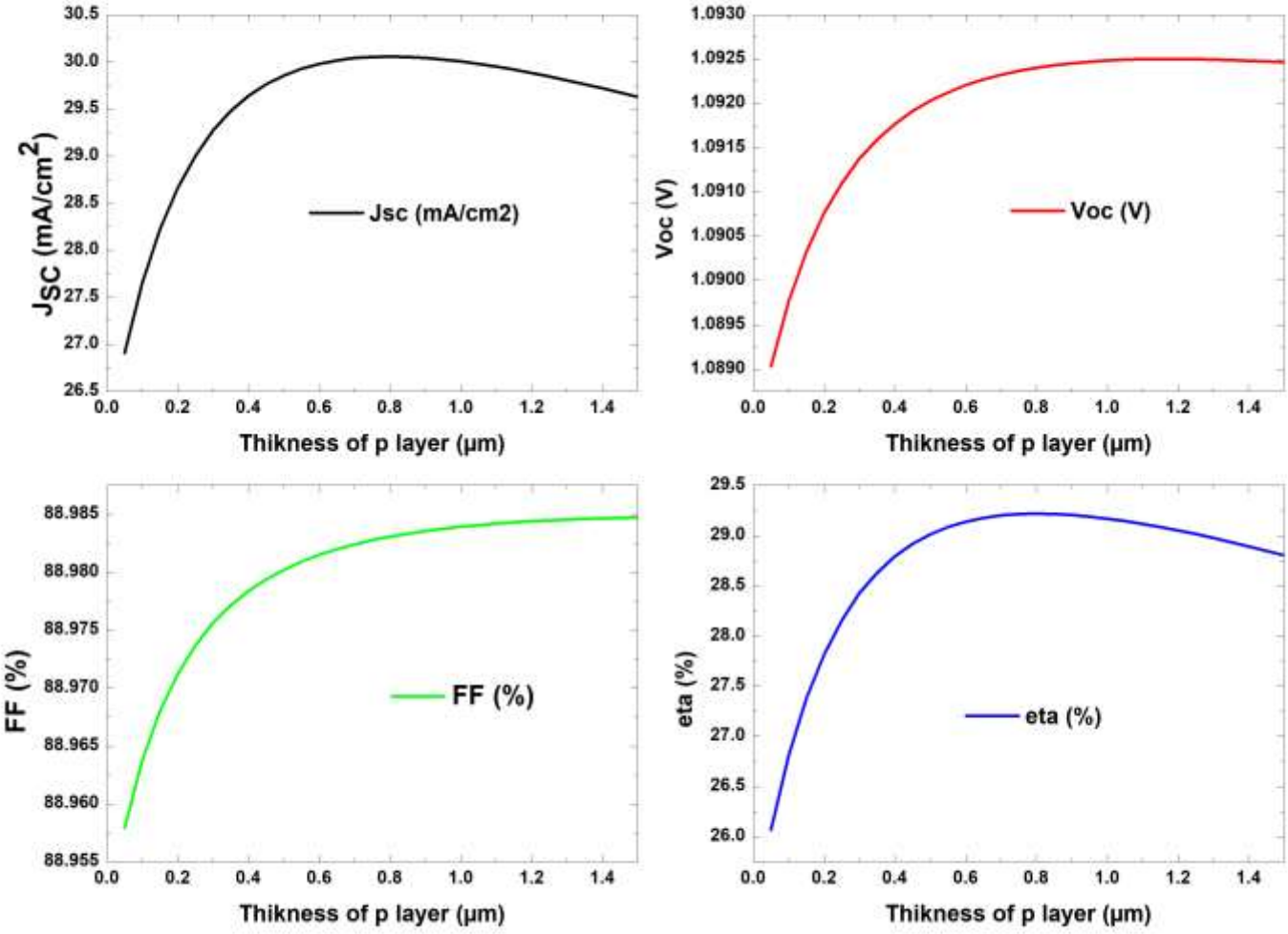

Figure 4.6 Simulated photovoltaic parameters of GaAs solar cell as function of thickness of the p-layer.

4.5.d Optimization of thicknesses of solar cell i-layer

As shown in Fig.4.7, with increasing i layer thickness from 0.5 μm to 3 μm, (*Jsc*,*Voc* and *FF* remains constant) The efficiency η increased slightly from 29.53 % to 29.82 %. The i-layer thickness of 3 μm may be considered an optimized value.

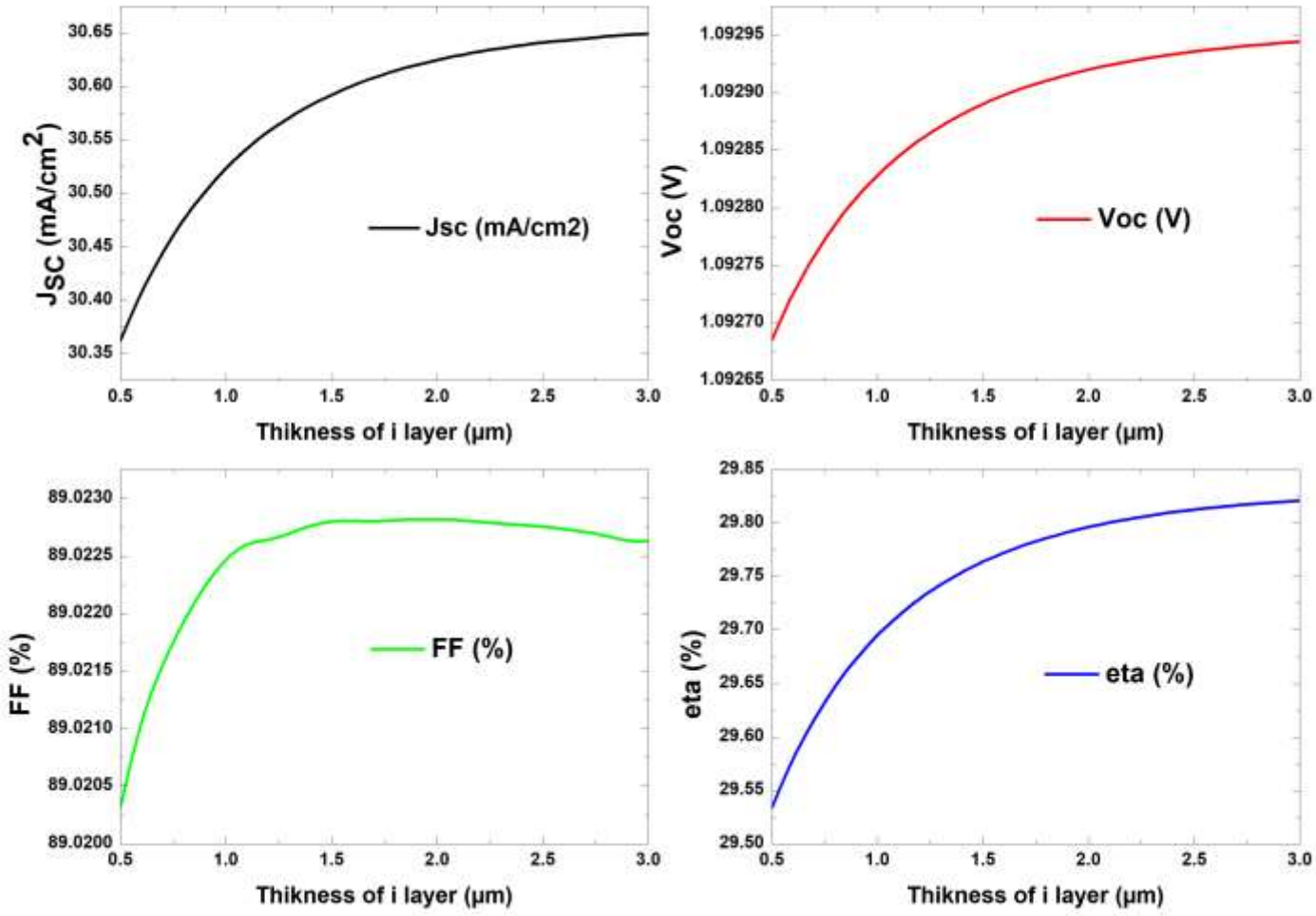

Figure 4. Simulated photovoltaic parameters of GaAs solar cell as function of thickness of the i-layer.

4.5.e Optimization of thicknesses of solar cell n-layer

As shown in Fig.4.8, with increasing n layer thickness from 0.5 μm to 2 μm, (*Jsc*,*Voc* and *FF* remains constant) The efficiency η increased from 29.82 %. To 30.04% The p-layer thickness of 2 μm considered an optimized value.

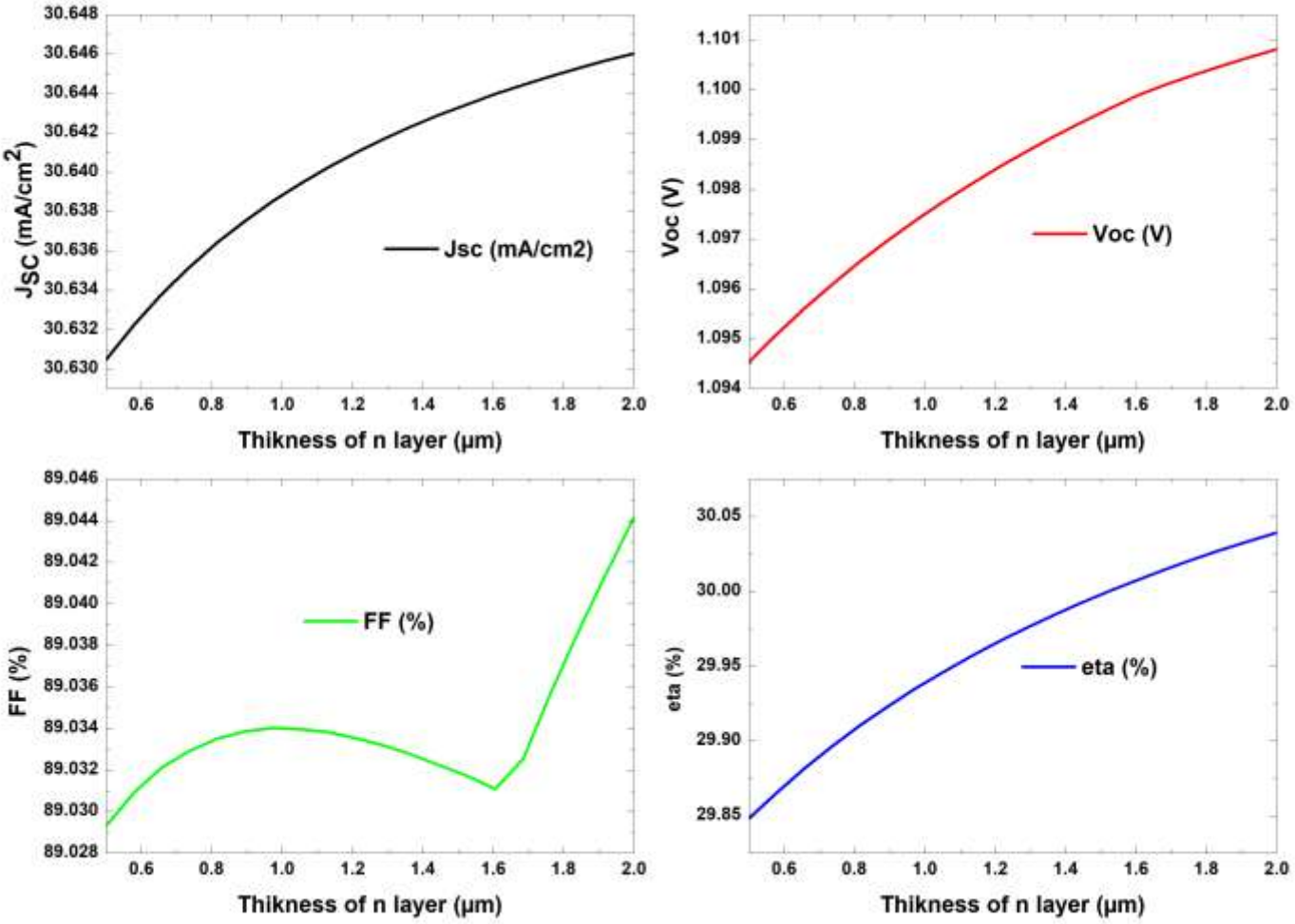

Figure 4.8 Simulated photovoltaic parameters of GaAs solar cell as function of thickness of the n-layer.

After improvement of J–V characteristic of GaAs solar cell by Optimization of acceptor and donor concentrations of p layer and n layer respectively and optimization of thicknesses of solar cell p, i and n layers. J–V characteristic of optimized GaAs solar cell is presented in figure 4.9. Table 4.3 shows the photo electrical parameters of optimized GaAs solar cell extracted from the corresponding J–V characteristic.

The electrical characteristics of the optimized GaAs solar cell obtained through simulation are, respectively, *Jsc*=30.64 mA/cm^2, *Voc*=1.10 V, *FF*=89.04 %, η=30.04 %.

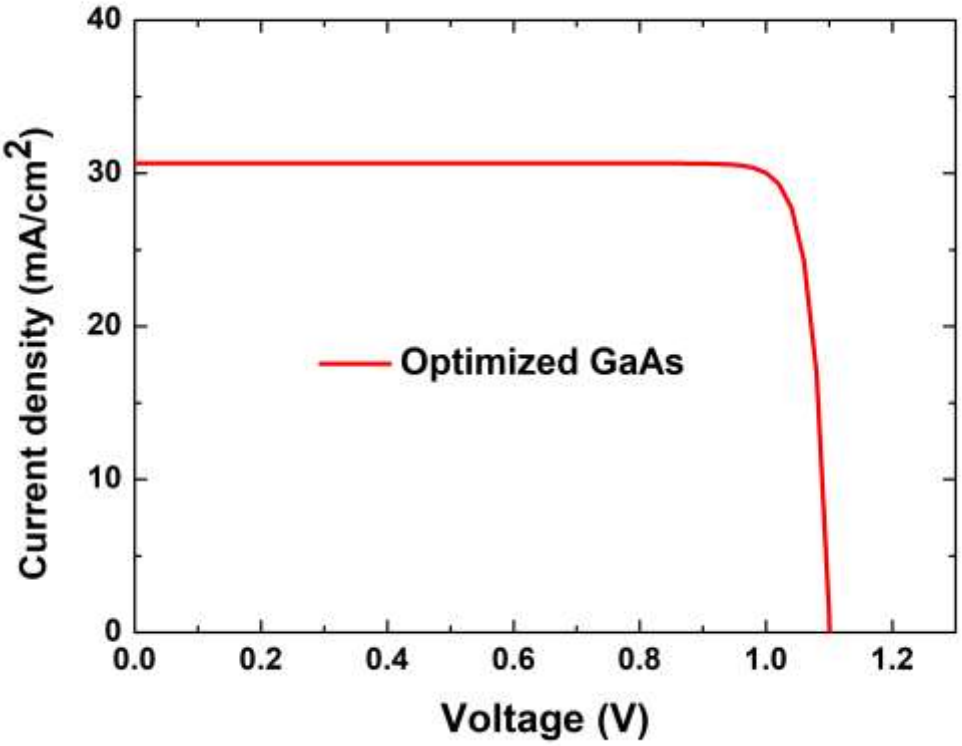

Figure 4.9 $J-V$ characterisitic of optimized p-i-n GaAs solar cell.

Table 4.3 Simulation and photovoltaic parameters of optimized GaAs solar cells.

	J_{sc}(mA/cm^2)	V_{oc}(V)	FF (%)	η (%)
p-i-n GaAs cell simulation	30.64	1.10	89.04	30.04

4.5 Conclusion

Through simulations, we examined the electrical characteristics of a p-i-n GaAs solar cell and identified important factors such as doping concentrations and layer thicknesses that significantly impact the performance of the device. By optimizing these parameters, we achieved notable improvements in efficiency, reaching up to 30.04%. This demonstrates the potential of GaAs solar cells to outperform traditional silicon-based solar cells, especially in environments where high performance and durability are critical.

The findings underline the importance of both material properties and careful structural optimization in pushing the efficiency limits of next-generation solar technologies.

Chapter 4 references

[1] Kayes BM, Nie H, Twist R, Spruytte SG, Reinhardt F, Kizilyalli IC, Higashi GS. 27.6% conversion efficiency, a new record for single junction solar cells under 1 sun illumination. Proceedings of the 37th IEEE Photovoltaic Specialists Conference, IEEE;2011.

[2] Green MA, Dunlop ED, Hohl-Ebinger J, Yoshita M, Kopidakis N, Hao X. Solar cell efficiency tables (Version 56).

[3] Yamaguchi, M. (2021). High-Efficiency GaAs-Based Solar Cells. IntechOpen.

[4] Cruz, A. G. G., Solís, M. D., González, L. G., Torres, J. H., López, M. L., Puente, G. C., ... & Peredo, L. Z. (2017). Theoretical study of c-GaN/GaAs single heterojunction solar cells. Matéria (Rio de Janeiro), 22, e-11887.

[5] Chahid, E., Nachaoui, M., Mir, Y., Amine, A., Kinani, M. A., Elrharib, A., ... & Zazoui, M. (2022). Numerical modeling of pin GaAs solar cell performance. Journal of Ovonic Research, 18(6).

[6] Singh, B., & Gupta, V. (2022). Impact of different parameters on the performance of GaAs solar cell using PC1D simulation. Materials Today: Proceedings, 62, 6407-6411.

[7] Pham, D. P., Lee, S., & Yi, J. (2022). Optimisation of four-terminal GaAs//Si tandem solar cells using numerical simulation. Materials Science in Semiconductor Processing, 139, 106365.

General Conclusion

The thesis provides a comprehensive exploration of semiconductor materials and solar cell technologies, highlighting their fundamental properties, operational principles, and optimization strategies.

Chapter 1 introduces the essential electronic properties of semiconductor materials, emphasizing the significance of crystal structures in determining their behavior. It sets the stage for understanding how materials like silicon, germanium, and gallium arsenide (GaAs) serve as the backbone of modern electronics and energy applications.

Chapter 2 delves into the fundamentals of solar cells, explaining the photovoltaic effect and detailing various types of solar cells. This chapter illustrates how solar energy is converted into electrical energy, emphasizing the advantages of different solar cell technologies, including emerging innovations.

Chapter 3 focuses on the SCAPS-1D simulation program, a tool for modeling and optimizing solar cell performance. It guides the reader through the program's functionalities, allowing for detailed simulations and analyses that aid in understanding the design and performance of solar cells.

Chapter 4 presents an in-depth study of GaAs solar cells, specifically their p-i-n structure. It covers the simulation of electrical characteristics, the impact of doping concentrations, and the optimization of layer thicknesses. The results demonstrate that through meticulous parameter adjustments, the efficiency of GaAs solar cells can be significantly enhanced, achieving efficiencies of up to 30.04%.

Overall, these chapters underscore the critical role of semiconductor materials in renewable energy technologies, particularly in solar cells, and highlight the importance of both material properties and careful design optimizations in advancing solar cell performance. The findings pave the way for developing next-generation solar technologies that could outperform traditional solutions, particularly in high-demand environments.